NASA TM-87679

NASA Technical Memorandum 87679 NASA-TM-87679 19860018641

CONTROL/STRUCTURES INTERACTION STUDY OF TWO 300 KW DUAL-KEEL SPACE STATION CONCEPTS

John W. Young, Frederick J. Lallman,
Paul A. Cooper, and Daniel P. Giesy

May 1986

NASA
National Aeronautics and
Space Administration

Langley Research Center
Hampton, Virginia 23665

ABSTRACT

This paper presents the results of an investigation of the influence of structural stiffness of the space station framework on the controllability of two 300 kw class, solar dynamic powered, dual-keel space station designs. The two design concepts differed only in the truss bay dimensions of the structural framework of the stations. Two control studies were made; (1) A study of the interaction of the framework structural response with the reaction control system used for attitude control during an orbital reboost maneuver; and (2) A study of the stability of the space station attitude control system with sensors influenced by the elastic deformations of the station framework. Although both configurations had acceptable control characteristics, the configuration with the larger truss bay dimension and its increased structural stiffness had more attractive characteristics for pointing control of the solar dynamic system during reboost and for attitude control during normal in-orbit operations.

SUMMARY

This paper presents the results of an investigation of the influence of structural stiffness of the space station framework on the controllability of two 300 kw class, solar dynamic powered, dual-keel space station designs. The two design concepts differed only in the truss bay dimensions of the structural framework of the stations. For one configuration the cubical bay size of the truss structure was 9 feet, and for the other it was 16.4 feet (Referred to as the 5-meter bay configuration).

Two control studies were conducted. The first was a study of the interaction of the framework structural response with the reaction control system used for attitude control during an orbital reboost maneuver. The second was a study of the stability of the space station attitude control system with sensors influenced by the elastic deformations of the station framework.

An analysis of the lower natural frequencies of the two configurations indicated that the framework frequencies of the 5-meter configuration were almost double those of the 9-foot bay configuration for corresponding modes. This increase results in a larger separation between the orbital reboost control system frequency and the lowest structural natural frequency and consequently a lower structural response during reboost for the 5-meter configuration.

During attitude control for in-orbit operations, instability can occur for both configurations when the disturbance excites higher structural modes involving large rotations of the module support region. A study of control stability using a compensated control law design to provide a positive stability margin for both configurations indicated that the 5-meter configuration has significantly larger gain margins than the 9-foot bay configuration, requires less structural damping to maintain a positive margin, is less sensitive to a change in model frequencies of the structure, and can respond more rapidly to commanded attitude changes.

INTRODUCTION

This paper presents the results from an investigation of the influence of structural stiffness of the space station framework on the controllability of a 300 kw class, solar dynamic powered, dual-keel space station. The purpose of the

investigation was to evaluate the attitude control characteristics of two space station concepts during normal in-orbit operations and during a controlled orbit reboost maneuver. The two design concepts differed only in the truss bay dimensions of the structural framework of the stations. The framework of the space station is composed of cubical bays. The first concept has a truss bay size of 16.4 feet (hereafter referred to as the 5-meter design) and the second station concept has a truss bay size of 9 feet (hereafter referred to as the 9-foot design). The definition of the space station designs and an investigation of their rigid body and structural dynamic characteristics are presented in reference 1. Only that information required for an understanding of the control study results is repeated in this paper.

Two control studies were conducted. The first was a study of an orbit reboost maneuver using reaction control system (RCS) jets to hold the attitude of the space station within given limits about the local vertical while applying a velocity increment along the flight path. Structural response of the station to the applied forces of the RCS was determined, and the interaction of the structural response with the control system was investigated. The second control study was concerned with the control moment gyro and attitude sensing system used to regulate the orientation of the space station during normal in-orbit operations. Frequency response (Bode) techniques were used to investigate the stability of the attitude control system with the effect of the dynamic response of the structure at the sensor location included.

Since the primary concern of the study was the effect of different truss bay sizes on the control aspects of the space station, the two space station configurations studied were designed to be as identical as possible in terms of overall dimensions, as well as in the mass and location of all payloads and subsystems. The dual-keel space station concept was in the definition phase at the time of this study and compromises affecting keel spacing, overall dimensions, structural components, and material properties were made between existing concepts that were under development by the two primary contractors concerned with the truss structure definition (Rockwell International and McDonnell Douglas). Since final dimensions were not established at the time of this study, neither configuration used in this study is an approved 300 kw class NASA reference configuration.

DEFINITION OF THE SPACE STATION CONFIGURATIONS

Dimensions of the 5-meter bay and 9-foot bay configurations studied are shown in figure 1, and their mass properties are given in Table I. As can be seen, the dimensions, masses, and mass inertias of the two space station configurations were formulated so that their rigid body characteristics would match as closely as permitted by the truss bay size differences. For example, the total keel length differed by only 4 percent, the total mass differed by only 0.2 percent, and the largest principal mass moment of inertia differed by only 2.4 percent. Reference 1 gives a description of masses and locations of payloads, power systems, heat rejection radiators, and other subsystems. The structural properties and dimensions of the truss components and support structures are also given in reference 1.

The control sensors and the control moment gyros constitute the attitude control assembly (ACA). These sensors and gyros are co-located at the origin of the coordinate system shown in figure 1. The RCS thrusters used for orbit reboost were located such that y-axis pitching moment arms were approximately the same for both configurations. They differed by 6 percent for the upper keel thrusters and only

1.2 percent for the lower keel thrusters. As can be determined from the information in Table I, the upper and lower keel thrusters are not located at the same distance along the y-axis from the center of mass of the station. Thus, during a reboost maneuver with all thrusters active, an unbalanced moment about the y-axis will occur causing the station to rotate away from its vertical position.

The 300 kw class station contains four habitation modules, four laboratory modules, two logistics modules, and a Japanese module (Fig. 2a). The modules are attached to a dog-bone shaped truss beam constructed normal to the y-z plane at the bay located at the origin of the coordinate system (Fig. 1). The centerlines of the modules, the module attachment truss beam, and its position relative to the keels, cross beams and the ACA are shown in figure 2b.

The station is powered by eight solar dynamic systems located on support structures attached to the transverse beam. A typical solar dynamic system is shown in figure 3a. The direction of the symmetric axis of each of the solar dynamic systems must be held to within 0.1 degrees of the solar vector for maximum operational efficiency. No attempt was made in the study to include the local elastic behavior of the solar dynamic system. An equivalent mass distribution system (shown in figure 3b) was used to represent the solar dynamic unit.

A detailed finite element model of the framework of each concept was developed to determine the natural modes and frequencies of the station concepts. The models are shown in figure 4 (see Ref. 1 for details). A finite element equation solver was used to evaluate the first 60 natural modes and frequencies of each configuration. A comparison of the natural frequencies below 0.4 hz is given in figure 5. A brief description of the first 15 modes are given in Table II and are referenced to figure 5 by letter.

REBOOST CONTROL SYSTEM STUDY

Because of atmospheric drag, the Space Station must be periodically reboosted to maintain a desired orbit. This maneuver is performed using four constant thrust reaction control system (RCS) jets. The purpose of the reboost control system is to maintain attitude control during the maneuver. The mechanics of the reboost maneuver and the assumed control logic will now be discussed.

Description of Reboost Control System

The four 75-pound, constant thrust RCS jets are located as shown in figure 1 with two jets above and two below the center of gravity of the station. The RCS jets are aligned with the x-axis of the station such that the thrust is in the orbital direction. The reboost system operates either with all four jets on or using only the upper jets. The resultant y-axis torques about the center of gravity of the station are given in Table III-A for the 5-meter and 9-foot stations for both the four and two jets on conditions. The differences in torque levels shown in Table III-A for the two configurations result from the small differences in center of gravity and thruster locations (see in Table I).

The reboost control logic is shown in figure 6. The logic is designed to off-modulate the lower RCS jets to hold the pitch attitude (θ_y) of the station within a one-degree deadband from the local vertical while applying the desired velocity increment along the flight path. The deadband, hysteresis, and pitch rate gain

values shown on figure 6 are the same as those of reference 2. It should be noted that only y-axis control is considered in the present analysis since the primary disturbance on the station during reboost is about this axis.

Rigid body pitch, pitch rate, and the associated torque history are shown in figure 7 for a typical reboost maneuver using the 9-foot configuration. The maneuver is initiated with the station aligned along the local vertical (θ_y=0°) by firing all four RCS jets. The resultant positive torque causes the station to rotate away from the vertical as shown in figure 7a. When the error signal ($E=\theta_y + k\dot{\theta}_y$) exceeds the deadband plus the hysteresis (1.05°), the lower jets are shut off, producing a negative torque about the station center of gravity. The negative torque condition is maintained until $E \leq 1°$ at which time all jets are again activated. This off-modulation of the lower jets is continued until the station reaches a limit cycle condition about the 1° bias or attitude error. The limit cycle condition occurs at about 1000 seconds in figure 7 and is characterized by periodic control switches and constant peaks in pitch and pitch rate as shown. The limit cycle characteristics for the 5-meter and 9-foot models are given in Table III-B.

The stability of the reboost control system and the limit cycle are illustrated on the pitch, pitch rate phase plane plot of figure 7c. The inward spiral to the limit cycle indicates a stable system. In the limiting condition, switches occur at θ_y=1.025° and $\dot{\theta}_y = \pm 0.025°$/sec.

The previously described reboost maneuver considered only rigid body dynamics. The following section of the report addresses control concerns from a flexibility standpoint.

Control Concerns Due to Flexibility

The switching logic shown in figure 6 requires y-axis pitch attitude and pitch rate. These quantities are obtained from sensors. The ideal situation would be for the sensors to output pure rigid body variations in θ_y and $\dot{\theta}_y$ for use in the control switching logic. However, in actual practice, the sensor signal will also contain flexible contributions to θ_y and $\dot{\theta}_y$. Thus, flexible interference at the sensors is of interest from a control standpoint.

A second control concern involves motion of the solar dynamic collectors (Fig. 3) during a reboost maneuver. As previously described, variations of the sun-line axis at the solar dynamic units must not exceed 0.1° for maximum efficiency of operation of the units.

Results and Discussion

Comparisons will now be given between the 5-meter and 9-foot stations with respect to flexibility at the sensor and solar collector locations during reboost maneuvers. Two control situations will be examined. In one case, the RCS switching logic (Fig. 6) is based on rigid body pitch and pitch rate. This would correspond to the use of ideal sensors since no flexible interference is present in the sensor outputs. In the second case, the actual sensor outputs which include both rigid body and flexible contributions are used in the control logic.

Typical time history responses will be presented to illustrate flexible effects at the sensor and solar collector locations. With one exception, the time history

responses presented are limited to those using a rigid body control logic since responses using sensor outputs for control are very similar in nature. This similarity will be illustrated with tabular comparisons of peak values for flexible variations obtained using both control techniques. The response results presented include contributions from the first 44 flexible modes as given in reference 1. This represented a frequency range from about 0.08 to 1.2 hertz for the 5-meter model and from about 0.06 to 0.72 hertz for the 9-foot model.

Sensor Location Responses.- Time history response comparisons of the 5-meter and 9-foot models are given in figures 8 through 13 for the first 500 seconds of a reboost maneuver. The histories include various combinations of rigid body and flexible y-axis pitch and pitch rate as measured at the sensor location. The responses were calculated using rigid body dynamics in the reboost switching logic but are typical of those for which the actual sensor outputs were used in the control logic.

Control histories for the responses of figures 8-13 are similar to that shown in the first 500 seconds of figure 7-d. Actual switching times are given at the top of Table IV. As previously discussed, the variations in switching times for the two models result from the small differences in mass properties (Table I). Switching times using sensor output for control are also given on Table IV. As expected, the switching times using actual sensor outputs are slightly different from those using a rigid body control logic.

Figure 8 shows that the flexible contribution to θ_y for the 5-meter model is about one-fourth that for the 9-meter station. This is illustrated in figure 9 by smaller flexible deviations from the rigid body motion in the 5-meter results. Figures 10 and 11 show larger flexible interference in pitch rate for the 9-foot model with the 5-meter flexible deviations being about one-half those for the 9-foot model.

Figure 12 shows the flexible contribution to the error signal for the two models. Flexible effects for the 5-meter are about one-third those for the 9-foot model. The flexible error signal deviations for the 9-foot model (Fig. 12-b) could be reason for concern when actual sensor output is used in the control switching logic since the -0.03 degree peak at about 383 seconds represents 60 percent of the 0.05° hysteresis used in the logic. However, no adverse effects were noted when actual sensor outputs were used for control since the error signal peaks occurred after switches (and were much lower before switches) and since the total error signal (Fig. 13) was relatively smooth in the 1 to 1.05 degree range involved in the switching logic. Nevertheless, with flexible deviations such as those shown in figure 12-b, the potential exists for deterioration of the hysteresis switching loop given in figure 6, and in actual practice, the reboost control error signal should be filtered to reduce flexible contributions at the sensors.

Phase plane representations of the previously described responses are given in figure 14. Note the larger flexible variations for the 9-foot station.

All response results to present have used a rigid body error signal ($\theta_{y_{RB}}$ and $\dot{\theta}_{y_{RB}}$) for control switching since they are typical of those obtained using actual sensor outputs for control. For example, figure 15 shows the total flexible error signal obtained when actual sensor output was used in the control logic. Comparisons of figure 15 with figure 12 shows no dramatic differences in the response results. The major difference occurs for the 9-foot model with peak flexible motions being smaller when sensor output control is used.

An important point should be made concerning the previously discussed responses. Note that the 5-meter responses are at a higher frequency than those for the 9-foot model. This has control implications in that the reboost control system frequency and the structural frequencies have a greater separation for the 5-meter station. For example, the lowest fundamental, y-axis structural framework mode (reference 1) occurs at 0.124 hertz for the 5-meter model and at 0.062 hertz with the 9-foot model. The limit cycle control frequency for both models is 0.014 hertz (Table III). Therefore, the control frequency is separated from the structural frequencies by a factor of about 9 for the 5-meter model and only about 4 with the 9-foot model. This larger separation for the 5-meter station should result in smaller control/structure interactions than with the 9-foot model.

Sensor location response summary.- A summary of the flexible response results for motions occurring at the sensor location is given in Table V. Peak response comparisons between the 5-meter and 9-foot stations are given for cases using both rigid body and sensor output control logic. The table includes the previously discussed y-axis results along with peak deviations in attitude and attitude rate about the other axes. Also shown are peak flexible values for position and acceleration at the sensor location. Note the general trend of reduced peaks when actual sensor outputs are used for control. Also, note that the sensor output and rigid body control results are generally closer for the 5-meter model than with the 9-foot model. This fact, along with the lower peaks attained for the 5-meter model, indicated a lower level of control/structure interaction than that achieved with the 9-foot station.

Solar collector responses.- Time history responses of sun-line variations at the outer solar dynamic collector unit (Fig. 3) are given in figures 16 through 19 for the 5-meter and 9-foot models during a reboost maneuver. As previously mentioned, the sun-line axis of the collector must be maintained within 0.1° of the solar vector for efficient operation of the unit. The responses shown in figures 16-19 were for a rigid body control switching logic.

The flexible contributions to y-axis pitch at the collector are given in figure 16. Both responses are within the 0.1° requirement, with the 5-meter peak being about one-fourth that attained on the 9-foot model. Figure 17 shows total y-axis pitch angle variations during the reboost. Due to the one-degree offset requirement during reboost, total y-axis pitch always exceeds the pointing requirement. However, if the rigid body pitch angle were known, it could be nulled using rotary joints on the transverse boom of the space station.

Figure 18 shows flexible variations of the out-of-plane component (θ_z) of the sun-line during reboost. As expected, these are smaller than the in-plane vibrations. Figure 19 illustrates the reduced flexible sun-line variations for the 5-meter station. The figure shows a continuous trace of the flexible sun-line at the outer solar collector during reboost.

Solar collector response summary.- A summary of response results at the solar collectors is given in Table VI for the 5-meter and 9-foot models. The results include the previously discussed motions at the outer collector as well as corresponding motions at the inner collector (Fig. 1). Shown are peak flexible values for attitude, attitude rate, position, and acceleration for cases using both a rigid body and a sensor output control switching logic.

As expected, peak motions at the inner collectors are smaller than at the outer collectors. Inner collector peak motions follow the same trends with respect to station truss bay size as previously discussed for the outer collectors.

Limit cycle responses.- Previous results have included responses during the initial 500 seconds of reboost maneuvers. Since the limiting condition (Fig. 7c) has not been attained at this point, it is of interest to examine motions during limit cycle operations.

Figure 20 shows y-axis pitch and pitch rate responses at the sensor location during the limit cycle for the 5-meter station. The flexible pitch (Fig. 20a) and pitch rate (Fig. 20b) limit cycle responses should be compared with the corresponding responses given in figures 8a and 10a for the initial phase of the reboost. The comparison shows that the peak limit cycle excursions are somewhat lower than those attained during the initial phase of the reboost. The phase plane plots of figures 20c and 20d indicate stability during the limit cycle.

Limit cycle comparison results are given in Table VII for the 5-meter and 9-foot models. Included are peak flexible values for $\theta_{y_{flex}}$ and $\dot{\theta}_{y_{flex}}$ at the sensors using both rigid body and sensor output control. Comparisons of Table VII with corresponding results in Table V show the reduced levels of the response during the limit cycle.

It should be noted that the previously described limit cycle results were obtained by initiating the time history responses at the proper value for rigid body pitch and pitch rate (for example, $\theta_{y_{RB}}$=1.025°, $\dot{\theta}_{y_{RB}}$=.025 deg/sec) and by assuming that the initial conditions on the flexible variables were zero. This is an approximation since in an actual reboost the flexible variables would have non-zero initial conditions in the limiting condition. This procedure was used to reduce computational requirements since a complete reboost to the limit cycle involves thousands of seconds of real time (Fig. 7).

Summary of Results from Reboost Control Analysis

Reboost control/structure interaction results from a comparison study of 5-meter and 9-foot space station models can be summarized as follows:

1. The higher fundamental structural frequency for the 5-meter model give a greater separation between reboost control system and structural mode frequencies than for the 9-foot model.

2. Flexible interference in sensed attitude for the 5-meter model is one-fourth that for the 9-meter model.

3. Flexible interference in sensed attitude rate for the 5-meter model is one-half that for the 9-foot model.

4. Flexible sun-line variations at the solar collectors for the 5-meter model are one-fourth those for the 9-foot model.

5. Flexible sun-line variations at the solar collectors are within a 0.1° pointing requirement for both station models.

6. Although an unfiltered attitude, attitude rate error signal produced satisfactory control system performance during reboost, a filtered signal is recommended.

ATTITUDE CONTROL SYSTEM STUDY

This section presents an analysis of the attitude control assembly (ACA) and the influence of truss size selection upon its performance. The attitude control system is designed to regulate the orientation of the space station to keep its longitudinal axis (z-axis) aligned with the gravity vector and to keep its plane perpendicular to the velocity vector. The control system consists of attitude-sensing instrumentation, control moment gyros, and electronics to cause corrective control moments to be applied to the space station whenever it moves away from the commanded attitude. This system is used during normal on-orbit operations and is turned off during reboost maneuvers. Analysis of the control system stability is conducted using frequency response (Bode) plots.

Two control laws are examined: (1) angular error and rate are used to form a proportional plus differential (PD) feedback control law and (2) a first order lag is added to form a compensated PD control law. The control laws are examined for the 5-meter and the 9-foot space station configurations (Figs. 1a and 1b, respectively). The Bode plots are used to determine several indicators of performance of the control systems applied to the two space station configurations. The indicators are

(1) gain margins for the structural modes
(2) required structural dampings
(3) sensitivities of modal frequency changes
(4) control bandwidths.

Control Law Specification

The space station attitude control system consists of control loops designed to regulate the angular orientation of the space station relative to the three orthogonal axes (x, y, z) on figures 1a and 1b. Attitude angle and rate sensors and control moment gyros (CMG's) are co-located at the origin of the axis system which is near the space station's center of gravity (cg). This report discusses attitude control about the y-axis which is parallel to the long transverse boom. The analysis was not repeated for rotations about the x and z-axes since the purpose of the present study is to make comparisons between the two space station configurations. Moreover, similar analyses of control about the other axes are expected to give similar results.

The block diagram of the control law for the y-axis is shown in figure 21. The attitude angle θ_y responds to moments applied to the space station by the CMG's and external and internal disturbances. In the present study, the effects of structural vibrations are included in this angle. Attitude sensing instrumentation provides electronic representations of the attitude angle θ_{ys} and its rate of change. The sensed attitude angle is subtracted from the commanded attitude angle (θ_{yc}) to form an attitude error signal (θ_{ye}). The electronic controller mechanizes a control law, specified in the form of a transfer function, to produce a commanded control moment (M_{yc}) based on the error signal. The CMG generates control moments (M_y) according to the commanded moments to drive the attitude error towards zero. Disturbances are not considered in the present study and the commanded attitude is set nominally to zero. Also, the dynamic response characteristics of the sensor package and the CMG's are not considered. Hence, the sensed attitude angle and rate are exact, and the control moments produced by the CMG's are exactly those commanded.

The closed-loop bandwidth of the system is specified in reference 2 to be 0.01 Hz. Using the common definition of bandwidth, this means that the attitude response (θ_y) is 70.7 percent ($1/\sqrt{2}$) of a sinusoidally varying attitude command (θ_c) at 0.01 Hz and is greater at lower frequencies. The system must also be stable.

The first control law is designed considering only the rigid-body dynamics of the space station and ignoring, for the moment, the structural dynamics. The rigid-body dynamics are described by the transfer function

$$\frac{\theta_y}{M_y}(s) = \frac{1}{I_{yy}s^2} \tag{1}$$

where I_{yy} is the moment of inertia about the transverse (y) axis, and s is the Laplace transform variable. For the present study, a value of 3.721×10^9 lbf-sec^2-in. was used for I_{yy} (see Table I). The control law required to stabilize the rigid-body model of equation 1 is of the form

$$\frac{M_y}{\theta_{ye}}(s) = K's + K \tag{2}$$

This is a proportional-differential (PD) control law operating on the attitude angle. The actual implementation of equation 2 would involve using the sensed angular error and the sensed angular rate as follows:

$$M_{yc} = K\theta_{ye} - K'\dot{\theta}_{ys} \tag{3}$$

Combining equations 1 and 2 yields the characteristic equation for the rigid-body model with the PD control law.

$$I_{yy}s^2 + K's + K = 0 \tag{4}$$

This is a second order system which is stable if the gains K' and K are both positive. The undamped natural frequency (ω_n) and the damping ratio (ξ) are given by the following.

$$\omega_n = \sqrt{\frac{K}{I_{yy}}}$$

$$\xi = \frac{1}{2\omega_n}\frac{K'}{I_{yy}} \tag{5}$$

If the natural frequency and damping ratio are given, then the control law gains can be calculated by rearranging equations (5). That is

$$K = \omega_n^2 I_{yy}$$

$$K' = 2\xi\omega_n I_{yy} \tag{6}$$

The closed-loop transfer function of the system shown in figure 21 is calculated using equations 1 and 2 to be

$$\frac{\theta_y}{\theta_{yc}}(s) = \frac{K' s + K}{I_{yy} s^2 + K' s + K} \tag{7}$$

For sinusoidal inputs of frequency ω for θ_{yc}, the ratio of the amplitudes θ_y and θ_{yc} is the magnitude of equation 7 where s is replaced by $i\omega$. The system bandwidth is the frequency for which the ratio is $1/\sqrt{2}$ or 70.7 percent.

The bandwidth of the space station control system is specified to be 0.01 Hz. Since no damping specification is given, a value for damping ratio of 0.275 (27.5 percent) is used. An initial calculation was performed using equation 6 with ξ=0.275 and ω_n=0.01 Hz (converted to radian measure). These calculations result in an angle feedback gain of K=14,690,000 in.-lbf/rad and an angular rate feedback gain of K'=128,600,000 in.-lbf/rad-sec^{-1}. However, the bandwidth for this initial system is calculated (using Eq. 7) to be 0.0164 Hz, which is 1.64 times the required value. For this simple system, changes in the bandwidth are proportional to changes in the undamped natural frequency. Therefore, to reduce the bandwidth to the proper value of 0.01 Hz, the natural frequency used in the above calculations is reduced by the factor of 1.64 to 0.00612 Hz. Repeating the calculations yields an angle feedback gain of K=5,490,000 in.-lbf/rad and an angular rate feedback gain of K'=78,600,000 in.-lbf/rad-sec^{-1}.

Frequency Response (Bode) Plots

The previous section described the specification of a PD controller for the space station considering only the rigid-body dynamics and ignoring the effects of structural vibrations. This section applies the frequency response method to examine the effects of structural dynamics upon the operation of the PD control law. For both configurations of the space station being considered, it is found that the PD control interacts with the structural dynamics to cause some of the structural modes to be unstable.

Frequency response (Bode) plots are used to determine whether feedback control systems are stable, and if stable, provide indications of how stable they are. They can also be used to design compensation filters which can be added to the control law to improve the stability. The attitude control loop is shown schematically in the block diagram of figure 21. The stability of the system can be determined by calculating the frequency-dependent effects of each of the blocks (controller, gyro, etc.) upon signals circulating around the loop. Open-loop frequency response plots are calculated using the transfer function from the input of the controller, θ_{ye}, to the response of the feedback signal, θ_{ys}. The "gain" is customarily given in terms of decibels (dB) and the phase angle is given in terms of degrees. To determine the stability of the system, examinations must be made of (1) the gains at those frequencies for which the phase angle is ±180 degrees and (2) the phase angles at those frequencies from which the gains are unity (0 dB). If the gain is less than unity when the phase angle is 180 degrees, then the system would have a "gain margin" equal to the negative (in terms of dB) of the gain at the frequency of 180 degrees phase angle. If the phase angle is greater than 180 degrees when the

gain is unity, then the system would have a "phase margin" equal to the phase angle in excess of 180 degrees at the frequency of unity gain. If these margins are positive for all frequencies, then the closed-loop system is stable.

Frequency response plots using the PD controller with the 5-meter and the 9-foot space station models developed in reference 1 are presented in figures 22 and 23, respectively. Part (a) of these figures are plots of loop gain in terms of dB plotted against frequency on a log scale. Part (b) of these figures are plots of phase angle in terms of degrees plotted against frequency on a log scale. For these calculations, the damping ratios of the structural modes were set to 0.005 (0.5 percent).

The lower frequency portions of the frequency response plots are smooth and well-behaved. This frequency range is below the frequencies of the structural modes, and the plots are determined by the rigid-body dynamics, the moment of inertia (I_{yy}), and the control law. For frequencies below 0.0111 Hz, the gain plots are dominated by the rigid-body dynamics of equation 1 which appear as a straight line with a slope of -40 dB per decade of frequency. For frequencies above 0.0111 Hz, the differential feedback term (K's) replaces the proportional feedback term (K) as the dominate term in equation 2 which causes a change of the slope to -20 dB per decade. The phase angle transitions from -180 degrees to -90 degrees over this range of frequencies. The stability of the rigid-body mode is verified by observing that the gain is unity at a frequency of 0.00659 Hz (unity gain crossover frequency) on figures 22a and 23a and the phase is -149 degrees at 0.00659 Hz on figures 22b and 23b, yielding a phase margin of 31 degrees.

The higher frequency portions of the frequency response plots reflect the effects of including the structural dynamics in the space station models. Each vibrational structural mode causes a sharp increase in the gain at its frequency of vibration which appears on the gain plots as an upward-pointing resonant "spike." These spikes are accompanied by a sudden reversal of phase angle which appears on the phase plots as a steep change from +90 degrees to -90 degrees. Between the resonant peaks, sharp decreases in gain occur producing downward-pointing spikes on the gain plots accompanied by steep changes in phase angle from -90 degrees to +90 degrees. There are approximately 50 structural modes in the models being used. The effects of approximately 20 structural modes can be detected on the frequency response plots.

Because approximations were made in specifying the control system (ideal sensor, ideal CMG, co-located sensor and CMG) and unpredictable parasitic effects would be introduced into the system when it is actually implemented (lags in electronics, computational and signal processing delays), the calculated phase plots cannot be trusted to give accurate information in the higher frequency range where the structural modes are present. Therefore, determinations made in this report concerning the stability of the structural modes will use the assumption of "worst-case" phase angle and will rely solely on the gain plots.

The frequency response gain plot for the 5-meter space station configuration is given in figure 22a. This plot indicates two structural modes of concern: (1) a mode at 0.236 Hz with only 1 dB gain margin, and (2) a mode at 0.339 Hz which is unstable by 3 dB (a "negative" gain margin of -3 dB). These modes correspond to modes K and M on figure 5a. The gain plot for the 9-foot configuration is given in figure 23a. This plot indicates two unstable structural modes: (1) a mode at 0.126 Hz with -7 dB gain margin, and (2) a mode at 0.185 Hz with -6 dB gain margin. These modes correspond to modes K and M on figure 5b. These particular modes are so

prominent because of the proximity of the attitude control system to the module platform. The space station model used in the present study includes a number of high mass modules (habitat, laboratory, logistics, and experimental modules) attached to a "dog bone" shaped module platform as shown in figure 2. The module platform is attached to the center of the long transverse boom. This attachment point is also the location of the attitude control sensor package and the CMG's. Modes K and M are characterized by large rigid-body rotations of the module platform and module assembly about the y-axis. The attitude control package is located on a "node" of modes K and M which means that the attitude angle and rate sensors will produce large signals whenever these two modes are excited and that control moments produced by the CMG's can excite these modes. These effects combine to give the space station models high gains at the frequencies of modes K and M resulting in the large resonant spikes seen in figures 22a and 23a. A drawing illustrating the structural mode shape of mode M is given in figure 24.

Control Law Compensation

Since the PD control law designed above proved to result in unstable structural modes, a second control law was designed to correct the problem. The object of the redesign is to reduce the magnitude of the frequency response for the higher frequency range while maintaining the rigid-body bandwidth and damping ratio. This is accomplished by adding a first-order lag to the control law and adjusting the proportional and differential gains. The result is a "compensated PD" controller.

The form of the compensated PD controller obtained by appending a first-order lag to the PD controller of equation 2 is

$$\frac{M_y}{\theta_{ye}}(s) = \frac{K's + K}{s/p+1} \tag{8}$$

where p is the "break frequency" of the first-order lag. For frequencies greater than the value of p, the open-loop gain is reduced by the factor p/ω which causes the higher frequency portions of the gain plots, figures 22a and 23a, to be "broken downwards" from a slope of -20 dB per decade to -40 dB per decade. Since this reduces the open-loop gains at the frequencies of the structural modes, positive increments of gain margin are produced. However, the inclusion of the compensation changes the unity gain crossover frequency, affecting the system bandwidth, and, to a greater degree, decreases the phase angle at the crossover frequency, reducing the rigid-body phase margin and damping ratio. Therefore, the gains K and K' need to be adjusted to recover the rigid-body damping ratio and to meet the specified bandwidth. After a number of iterations of K, K', and p, the following set of values to be used in the compensated PD control law of equation (8) was obtained.

K = 3,390,000 in-lbf/rad

K' = 139,800,000 in-lbf/rad-sec^{-1}

p = 0.0582 rad/sec (0.00927 Hz)

Frequency response plots for the 5-meter and the 9-foot configurations using the compensated PD controller are given in figures 25 and 26, respectively. The lower frequency portions of the gain plots, figures 25a and 26a, have a change of slope from -40 dB per decade to -20 dB per decade at a frequency of 0.00386 Hz and a

change back to -40 dB per decade at a frequency of 0.00927 Hz. The phase increases to -156 degrees at 0.00598 Hz and then decreases back towards zero. The unity gain crossover occurs at 0.00598 Hz and the phase margin is 24 degrees. The closed loop natural frequency of the rigid-body mode is 0.00598 Hz, the damping ratio is 0.275, and the bandwidth, as required, is 0.01 Hz.

The addition of the compensation causes the higher frequency portions of the gain plots, figures 25a and 26a, to be decreased in gain and the phase angles to be decreased (lagged) by 90 degrees, figures 25b and 26b. The gain margins for the 5-meter configuration are increased to +24 dB and +23 dB for modes K and M, respectively. The gain margins for the 9-foot configuration are increased to +11 dB and +15 dB for modes K and M, respectively. Note that greater changes of gain margins, resulting from the addition of the compensation, occur for the higher frequency modes (see Table VIII). In general, the effectiveness of adding the compensation to the control law is more effective for the 5-meter configuration than for the 9-foot configuration because the frequencies of its structural modes are higher.

Comparison of Space Station Configurations

The frequency response characteristics of the two space station configurations are very similar since both stations were identical except for differing truss bay size. For each of the control laws studied, the low frequency characteristics (including the rigid-body dynamics) appear to be identical because the moments of inertia are nearly the same. The high frequency characteristics are similar with the major difference being that the frequencies of the structural modes of the 5-meter configuration are approximately twice those of the 9-foot configuration because of its greater stiffness. Comparisons made between the two configurations in this section can generally be attributed to this difference in stiffness.

The preceding sections have discussed the design of two control laws. The first is the PD control law which is the simplest that can stabilize the rigid-body dynamics of the space station, but which is unacceptable since unstable structural modes result for both the 5-meter and the 9-foot configurations. Any disturbance of these modes is detected by the attitude rate sensor which causes control moments to be produced by the CMG's. These moments are of sufficient strength to overcome the structural damping (0.5 percent) and cause the structural response to increase in amplitude. Higher resonant peaks for the 9-foot configuration, figure 23a, indicate that the amplitudes of its unstable structural modes would grow at a faster rate than for the 5-meter configuration, figure 22a.

The second control law studied is the compensated PD control law which is the simplest that can stabilize the rigid-body dynamics of the space station without destabilizing the structural modes. The compensated PD control law employs a first order, low-pass filter which attenuates the high frequency components of the signals being transmitted from the attitude rate sensor to the CMG's. Now, the moments produced by the CMG's in response to disturbances of the structural modes are not large enough to overcome the structural damping, resulting in stable structural modes. Comparisons of the two space station configurations will be made in the following discussion using the compensated PD control law. The results of these comparisons are summarized in Table IX.

Gain Margin.- Using the compensated PD control law, the critical mode for the 5-meter configuration is mode M with a gain margin of +23 dB. The critical mode for

the 9-foot configuration is mode K with a gain margin of +11 dB. The difference of 12 dB is in favor of the 5-meter configuration. A certain level of gain margin must be present in the actual operating system to insure stable operation with a reasonable decay rate for any structural mode that may be excited. Additional amounts of gain margin must be included in the control system design to account for (1) inaccuracies and engineering approximations made in the construction of the structural dynamics model, the sensor models, and the CMG models; (2) off-nominal performance of the structure, sensors, and CMG's; (3) design changes to the system, (4) varying payload complement; (5) computational and signal processing artifacts; and (6) aging of the system. The 5-meter configuration would be better able to accommodate any of the above items because of its greater gain margin.

Structural Damping.- The damping ratios of the structural modes were assumed to be 0.005 (0.5 percent) in the above analysis. This value is suspect because damping ratio is difficult to estimate with any degree of accuracy. The addition of damping to a structure is also a difficult task. However, the closed-loop stabilty of the space station depends on the amount of damping present in the structure. Since the gain margins are functions of the structural damping ratio, estimates of the damping ratios required to meet a specified gain margin can be calculated.

A sketch of an isolated structural mode is presented in figure 27. For this example, a structural mode having a damping ratio of 0.005 (0.5 percent) is shown with a gain margin of 26 dB. For lightly damped modes such as this one, the height of the resonant peak is inversely proportional to the damping ratio. For example, if the damping ratio is reduced by a factor of 4 to 0.00125, the height of the peak will increase by a factor of 4 (an increase of 12 dB) reducing the gain margin to 14 dB. If a gain margin specification of 20 dB were imposed on the system design, then the minimum damping ratio required to meet the specification would be 0.0025 in this example.

The structural damping ratios required to meet a hypothetical gain margin specification of 20 dB are calculated to be 0.34 percent for the 5-meter configuration and 1.5 percent for the 9-foot configuration, both using the compensated PD control law. This means that the 5-meter configuration requires several times less structural damping than the 9-foot configuration to meet a given gain margin specification.

Structural Frequencies.- Over the lifetime of the space station, several changes to the structural dynamic characteristics will occur. Payloads will be attached and deployed. The space shuttle will dock and undock. New structural members and devices may be added to the space station during future growth. Aging of the structural components from being exposed to the space environment of earth orbit for periods of decades may result in changes in the structural stiffness. Each of these items affects the structural modes and their natural frequencies. The gain margins are related to the frequencies of the structural modes. Estimates of the change of gain margin caused by changes in the structural frequencies can be calculated.

A sketch of an isolated structural mode is presented in figure 28. For changes in frequency of the mode, the resonant peak moves along a sloping line. The slope is -20 dB/decade for the PD control law (as shown) and is -40 dB/decade for the compensated PD control law. For this example, the mode has a frequency of ω_n and a gain margin of 26 dB. If, for example, the frequency were reduced by a factor of 10 (one decade), the gain would increase by 20 dB, resulting in a new gain margin of 6 dB. If a gain margin specification of 20 dB were imposed on the system design,

then the minimum frequency of the structural mode required to meet the specification would be one half of ω_n. The frequency of the mode can be changed by -50 percent in this example.

The changes of the structural frequencies which would result in instability (0 dB margin) are calculated to be -75 percent for the 5-meter configuration and -47 percent for the 9-foot configuration, both using the compensated PD control law. The 9-foot configuration becomes unstable if the structural frequencies are halved whereas the 5-meter configuration remains stable until the frequencies are reduced by a factor of 4. This means that the 5-meter configuration can tolerate larger reductions in the structural frequencies than the 9-foot configuration.

System Bandwidth.- The bandwidth of a system is a measure of its responsiveness to changes of commanded operating condition (in the case of the space station, the commanded attitude) and the speed at which the effects of disturbances are corrected. The control laws designed in the present study meet a bandwidth specification of 0.01 Hz. Given a different bandwidth specification, the parameters of the control laws would be different, resulting in new levels of gain margin for the structural modes. If, on the other hand, a gain margin specification were given for the structural modes of the space station, different sets of parameters for the control laws would be required for the two space station configurations, resulting in different bandwidths.

A sketch of an isolated structural mode is presented in figure 29. The linear portions of the frequency response shown are functions of the controller gains and the moment of inertia of the space station. The system bandwidth is generally proportional to the unity gain (0 dB) crossover frequency. The bandwidth is proportional to the values of the gains (specifically, the dominant gain in the region of the crossover) and is inversely proportional to the moment of inertia. If the moment of inertia were increased by the addition of payloads, the bandwidth would decrease indicating that the space station would be slower to respond to commanded attitude changes and disturbances. In order to maintain a specified bandwidth, the controller gains must be increased in inverse proportion to the change of the inertia. This effect is common to both space station configurations. The addition of payloads also affects the structural modes. In order to calculate the effects on the gain margins, new structural dynamics models accounting for the changed payload configuration are required. This topic is beyond the scope of the present study and is left to future analyses.

If, on the other hand, the gains of the controller are increased, the system bandwidth increases. The resonant peak of the structural mode "rides" unchanged on the linear portion of the frequency response plot. The result is a reduction of gain margin of the structural mode associated with the increased bandwidth. The amount of the gain margin change relative to the change of bandwidth can be estimated from the slope of the frequency response plot at the crossover frequency. The slope is -20 dB per decade for the PD controller (as shown on figure 29) and -40 dB per decade for the compensated PD controller.

Given a hypothetical gain margin specification of 20 dB and using compensated PD controllers of the form of equation 8, the bandwidth of the 5-meter space station configuration is calculated to be 0.012 Hz and the bandwidth of the 9-foot configuration is 0.006 Hz. Since the 5-meter configuration has twice the bandwidth of the 9-foot configuration, it can respond to commanded attitude changes twice as fast and can recover from disturbances in half the time.

Conclusions from Frequency Response (Bode) Analysis

The frequency response characteristics of the two space station configurations are very similar with the major difference being that the frequencies of the framework structural modes of the 5-meter configuration are approximately twice those of the 9-foot configuration because of the greater stiffness resulting from its larger truss bay size. Conclusions from comparisons of the two configurations can generally be attributed to this difference.

1. The structural modes having the greatest potential for instability involve large rigid-body rotations of the module platform.

2. Compensation is required in the attitude controllers to insure stability of the structural modes.

3. The 5-meter configuration has significantly larger gain margins than the 9-foot configuration.

4. The 5-meter configuration requires a fraction of the amount of structural damping that the 9-foot configuration requires.

5. The 5-meter configuration can tolerate larger changes of the modal frequencies than the 9-foot configuration.

6. The 5-meter configuration can respond to commanded attitude changes and can correct disturbances faster than the 9-foot configuration.

CONCLUSIONS

This paper presents the results of an investigation of the influence of structural stiffness of the space station framework on the controllability of two 300 kw class, solar dynamic powered, dual-keel space station designs. The space station configurations differed in design only in the truss bay dimensions of the structural framework of the stations.

Two control studies were made. The first was a study of the interaction of the framework structural response with the attitude control system during an orbital reboost maneuver. The second was a study of the stability of the space station attitude control systems with sensors influenced by the elastic deformations of the station framework.

An analysis of the lower natural frequencies of the two configurations indicated that the framework frequencies of the 5-meter configuration were almost double those of the 9-foot bay configuration for corresponding modes. This increase results in a larger separation between the orbital reboost control system frequency and the lowest structural natural frequency for the 5-meter configuration. The structural response of the 5-meter bay configuration at the sensor location which contributed to the sensed attitude rate is one-fourth that of the 9-foot bay configuration. Attitude control using an unfiltered proportional plus differential feedback signal during reboost caused one-fourth less rotation of the sun-line axis of the solar dynamic system for the 5-meter configuration than for the 9-foot configuration.

The stability analysis of an unfiltered proportional plus differential attitude control system used to regulate the orientation of the space station during normal in-orbit operations indicates that instability can occur for both configurations when the disturbance excites higher structural modes involving large rotations of the module support region. A compensated control law was designed to provide a positive stability margin for both configurations. The 5-meter bay configuration has significantly larger gain margins than the 9-foot bay configuration and requires less structural damping to maintain a positive margin. The 5-meter configuration also is considerably less sensitive to a change in modal frequencies of the structure and with a higher control bandwidth can respond more rapidly to commanded attitude changes.

Although both the 5-meter bay configuration and the 9-foot bay configuration had acceptable control characteristics, the 5-meter bay configuration with its increased structural stiffness has more attractive characteristics for pointing control of the solar dynamic system during reboost and for attitude control during normal on-orbit operations.

REFERENCES

1. Dorsey, John T.; Sutter, Thomas R.; Lake, Mark S.; and Cooper, Paul A.: Dynamic Characteristics of Two 300 KW Class Dual Keel Space Station Concepts. NASA TM-87680, March 1986.

2. Space Station Reference Configuration Description. JSC-19989, August 1984.

TABLE I. MASS PROPERTIES OF THE DUAL-KEEL CONFIGURATIONS.

	9-foot	5-meter
CENTER OF GRAVITY (IN)		
	X = 123.1 Y = 45.5 Z = 126.4	X = 122.0 Y = 45.9 Z = 112.0
TOTAL MASS ($LBF-SEC^2/IN$)		
	M = 3329.5 (1,285,000 lbm)	M = 3334.0 (1,287,000 lbm)
MASS INERTIA MATRIX ($LBF-SEC^2-IN$)		
	IXX = 6.078E+9 IYY = 3.696E+9 IZZ = 3.618E+9 IXY = 8.337E+6 IXZ = 7.475E+7 IYZ = -7.010E+7	IXX = 6.226E+9 IYY = 3.721E+9 IZZ = 3.763E+9 IXY = 6.550E+6 IXZ = 7.174E+7 IYZ = -1.056E+8
LOCATION OF RCS THRUSTERS (IN)		
UPPER KEEL	X = 0 Y = 670.4, -670.4 Z = -1296.0	X = 0 Y = 828.2, -828.2 Z = -1378.0
LOWER KEEL	X = 0 Y = 670.4, -670.4 Z = 1944.0	X = 0 Y = 828.2, -828.2 Z = 1968.5

TABLE II. MODE SHAPE KEY

A - FIRST RADIATOR Y BENDING (OUT OF PHASE)

B - FIRST RADIATOR Y BENDING (IN PHASE)

C - FIRST TRANSVERSE BOOM Z BENDING (SYMMETRIC)

D - FIRST TRANSVERSE BOOM X BENDING (SYMMETRIC)

E - FIRST TRANSVERSE BOOM TORSION (SYMMETRIC)

F - FIRST TRANSVERSE BOOM TORSION (ANTISYMMETRIC)

G - FIRST RADIATOR Z BENDING (IN PHASE)

H - FIRST RADIATOR Z BENDING (OUT OF PHASE)

I - FIRST TRANSVERSE BOOM X BENDING WITH TORSION (ANTISYMMETRIC)

J - SECOND TRANSVERSE BOOM Z BENDING

K - FIRST KEEL Y BENDING

L - FIRST KEEL Y BENDING (ANTICLASTIC PLATE)

M - FIRST MODULE SUPPORT TORSION WITH UPPER KEEL Y BENDING

N - SECOND TRANSVERSE BOOM TORSION (SYMMETRIC)

O - SECOND TRANSVERSE BOOM TORSION (ANTISYMMETRIC)

TABLE III. REBOOST CONTROL SYSTEMS PARAMETERS

(a) Y-axis torque about center of gravity, ft-lb

	All RCS jets ON	Upper RCS jets ON
5-meter	4581	-18625
9-foot	4940	-17780

(b) Limit cycle characteristics

	Period, sec	Frequency, Hz	All RCS jets ON, sec	Upper RCS jets ON, sec
5-meter	73.6	.014	59.1	14.5
9-foot	69.6	.014	54.4	15.1

TABLE IV.- REBOOST SWITCHING TIMES USING RIGID BODY OR SENSOR OUTPUT FOR CONTROL, SEC

*Event	1	2	3	4	5	6	7	8	9	10
Rigid Body Control										
5-meter	48.79	72.07	162.85	184.38	268.58	288.62	367.26	386.05	460.10	477.87
9-foot	46.82	72.03	159.15	182.44	263.11	284.74	359.87	380.01	450.57	469.62
Sensor Output Control										
5-meter	48.88	72.33	164.46	186.41	272.78	293.40	374.43	393.88	470.99	489.54
9-foot	46.87	72.19	160.33	184.0	266.23	288.34	365.1	385.51	456.12	475.45

*Events indicate off/on modulation times for lower RCS jets. All jets are initially on. Lower jets are turned off at 1, 3, 5, 7, and 9. Lower jets are turned on at 2, 4, 6, 8, and 10.

TABLE V. SUMMARY OF PEAK FLEXIBLE RESPONSES OCCURRING AT SENSOR LOCATION DURING REBOOST MANEUVER USING RIGID BODY OR SENSOR OUTPUTS FOR CONTROL. (RSS value is the peak resultant occurring during the maneuver.)

	5 Meter		9 Foot	
	RCS logic based on		RCS logic based on	
	Rigid Body	Sensor Output	Rigid Body	Sensor Output
Attitude, deg				
θ_x	.001	Same	.004	Same
θ_y	.007	.006	.026	.018
θ_z	.003	Same	.013	.010
RSS	.007	Same	.026	.018
Attitude rate, deg/sec				
$\dot{\theta}_x$	.001	Same	.002	Same
$\dot{\theta}_y$	.007	Same	.014	.007
$\dot{\theta}_z$	.004	Same	.009	.006
RSS	.007	Same	.014	.009
Sensor Output, deg (k = 1 sec)				
$\theta_y + k\dot{\theta}_y$	.010	Same	.030	.021
Position, in.				
x	.080	.077	.260	.210
y	.012	.009	.036	.030
z	.040	.035	.089	.114
RSS	.080	.080	.260	.225
Acceleration, (g's x 10^{-5})				
a_x	31.0	31.3	29.5	23.9
a_y	6.8	Same	5.4	5.0
a_z	10.6	10.9	9.8	8.5
RSS	31.3	31.7	31.1	24.0

TABLE VI. SUMMARY OF PEAK FLEXIBLE RESPONSES OCCURRING AT THE OUTER AND INNER SOLAR COLLECTORS DURING REBOOST USING RIGID BODY OR SENSOR OUTPUTS FOR CONTROL (RSS value is the peak resultant occurring during the maneuver.)

	5 Meter				9 Foot			
	OUTER		INNER		OUTER		INNER	
	Rigid Body	Sensor Output	Rigid Body	Sensor Output	Rigid Body	Sensor Output	Rigid Body	Sensor Output
Attitude, deg								
θ_y	.023	.024	.015	Same	.091	.088	.062	.064
θ_z	.018	.014	.016	.012	.047	Same	.042	Same
RSS	.024	Same	.018	.016	.092	.10	.067	.082
Attitude rate, deg/sec								
$\dot{\theta}_y$	.023	.022	.012	Same	.042	.40	.026	Same
$\dot{\theta}_z$	.014	.013	.012	.009	.021	.16	.019	.016
RSS	.024	Same	.013	.012	.043	.44	.029	.030
Position, in.								
x	.72	.54	.35	.27	2.03	2.41	1.23	1.46
y	.14	.12	.12	.10	.36	.48	.31	.41
z	.29	.24	.13	.10	.95	1.39	.41	.63
RSS	.73	.54	.35	.28	2.19	2.78	1.30	1.61
Acceleration, (g's x 10^{-5})								
a_x	162.4	112.2	56.2	55.8	121.8	116.0	53.9	56.8
a_y	32.1	32.0	25.6	24.2	33.1	32.5	21.5	24.8
a_z	51.8	47.2	26.2	25.7	48.9	51.5	26.1	31.4
RSS	163.2	122.3	58.8	58.9	122.0	126.8	54.4	63.0

TABLE VII. COMPARISON OF PEAK FLEXIBLE RESPONSES OCCURRING AT SENSOR LOCATIONS DURING LIMIT CYCLE PHASE OF REBOOST MANEUVER.

	5 Meter		9 Foot	
	RCS logic based on		RCS logic based on	
	Rigid Body	Sensor Output	Rigid Body	Sensor Output
θ_y, deg	.006	Same	.017	Same
$\dot{\theta}_y$, deg/sec	.006	Same	.008	Same

TABLE VIII. STRUCTURAL MODE GAIN MARGINS *

	PD Control Law	Compensated Law
5-meter		
K (0.236 Hz)	+1 dB	+24 dB
M (0.339 Hz)	-3 dB	+23 dB
9-foot		
K (0.126 Hz)	-7 dB	+11 dB
M (0.185 Hz)	-6 dB	+15 dB

*Negative gain margins indicate unstable modes.

TABLE IX. SPACE STATION CONFIGURATION COMPARISONS *

	5-meter	9-foot	Comments
Minimum Gain Margin	23 dB	11 dB	12 dB advantage for 5-meter configuration
Structural Damping Required for 20 dB Margin	0.34%	1.5%	5-meter requires 4-5 times less damping
Modal Frequency Change for Instability	-75%	-47%	5-meter is more tolerant of frequency changes
Maximum Bandwidth for 20 dB Margin	0.012 Hz	0.006 Hz	5-meter attitude control is twice as responsive

*Compensated PD Controller

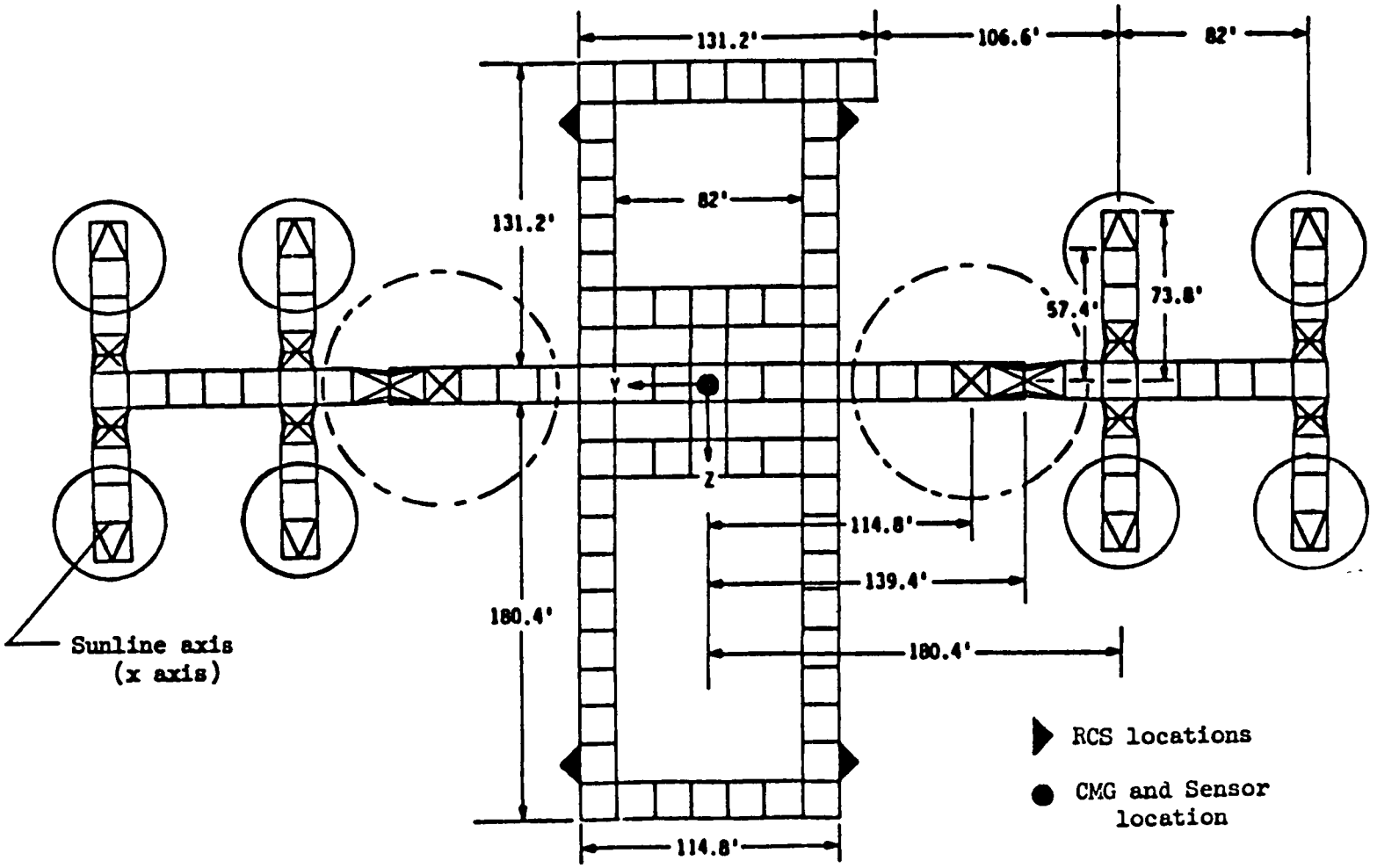

Figure 1a.- Schematic of dual-keel 300kw space station with 5-meter bay size truss structure.

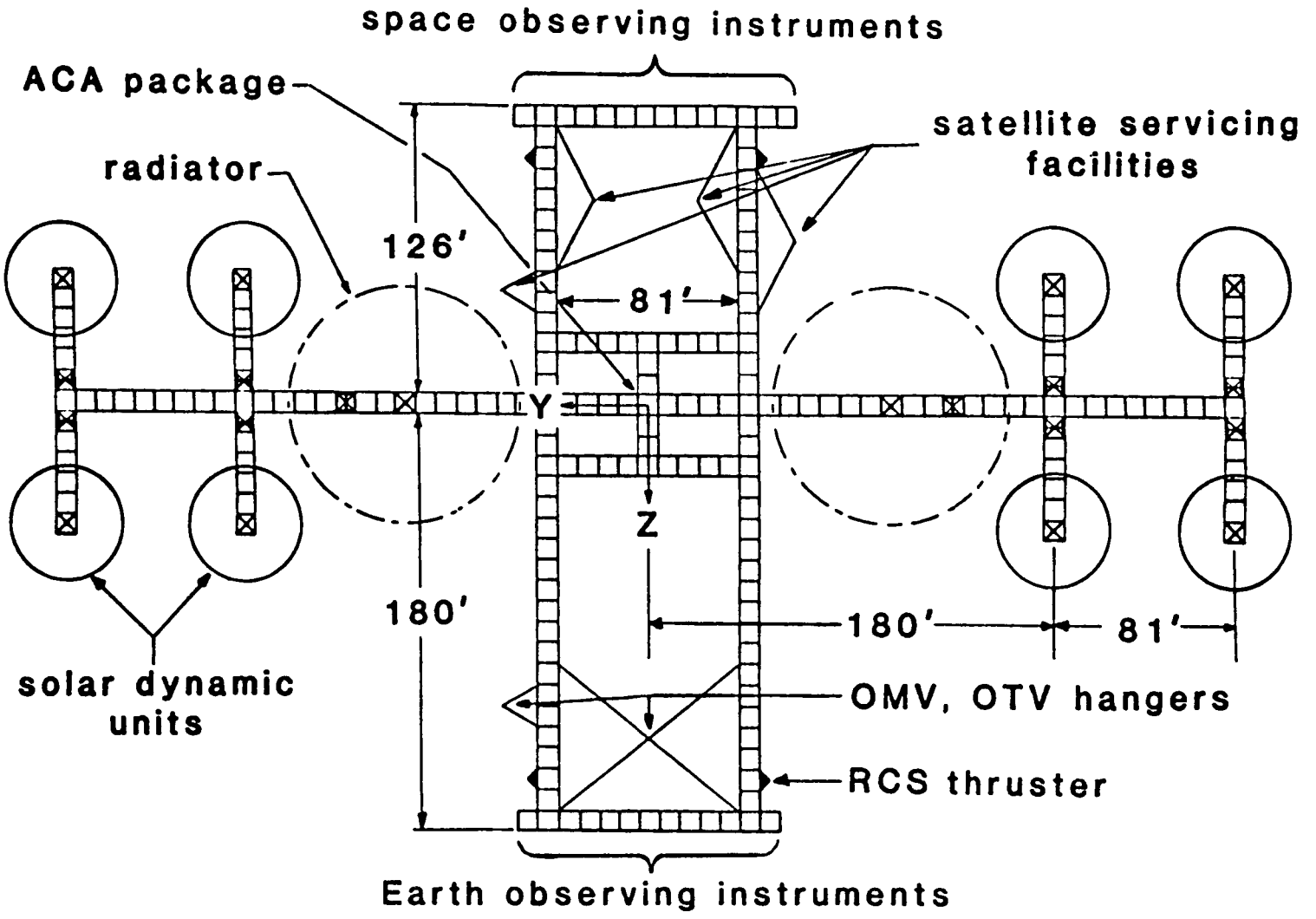

Figure 1b.- Schematic of dual-keel 300kw space station with 9-foot bay size truss structure.

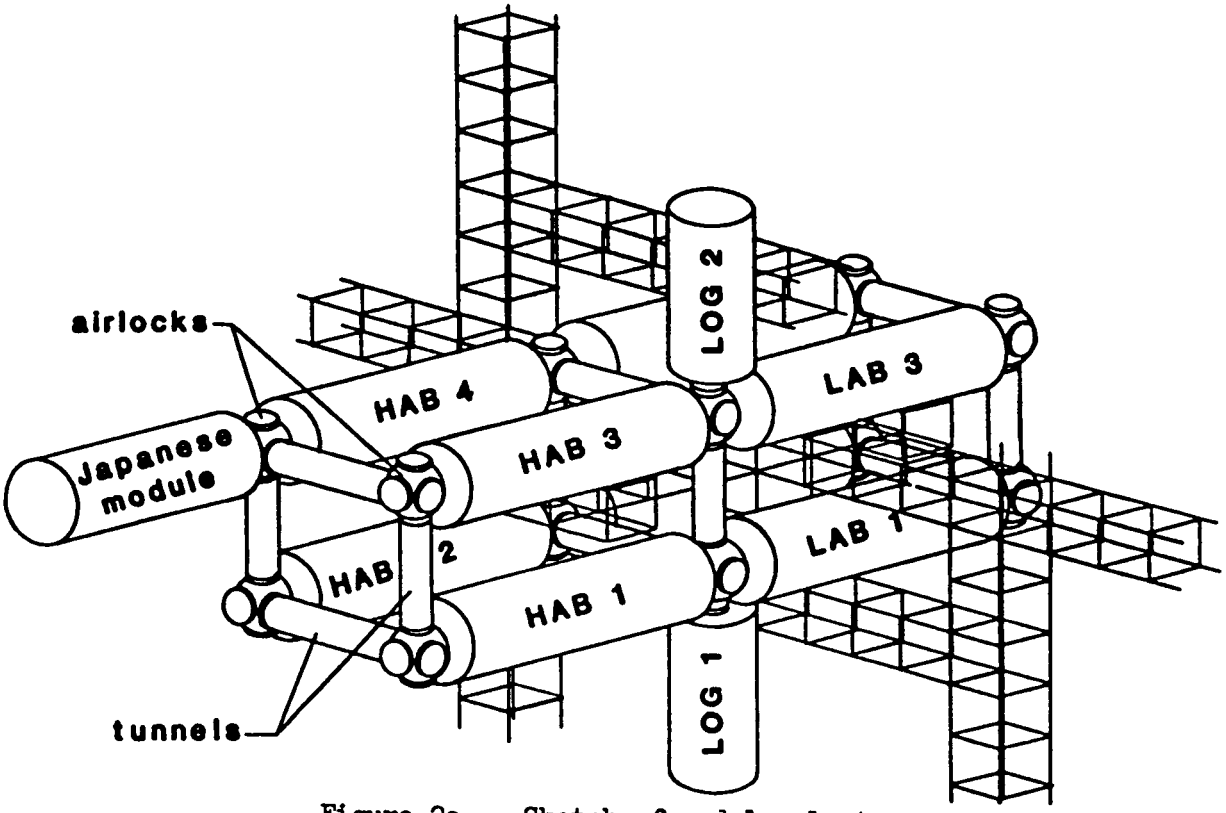

Figure 2a.- Sketch of module cluster.

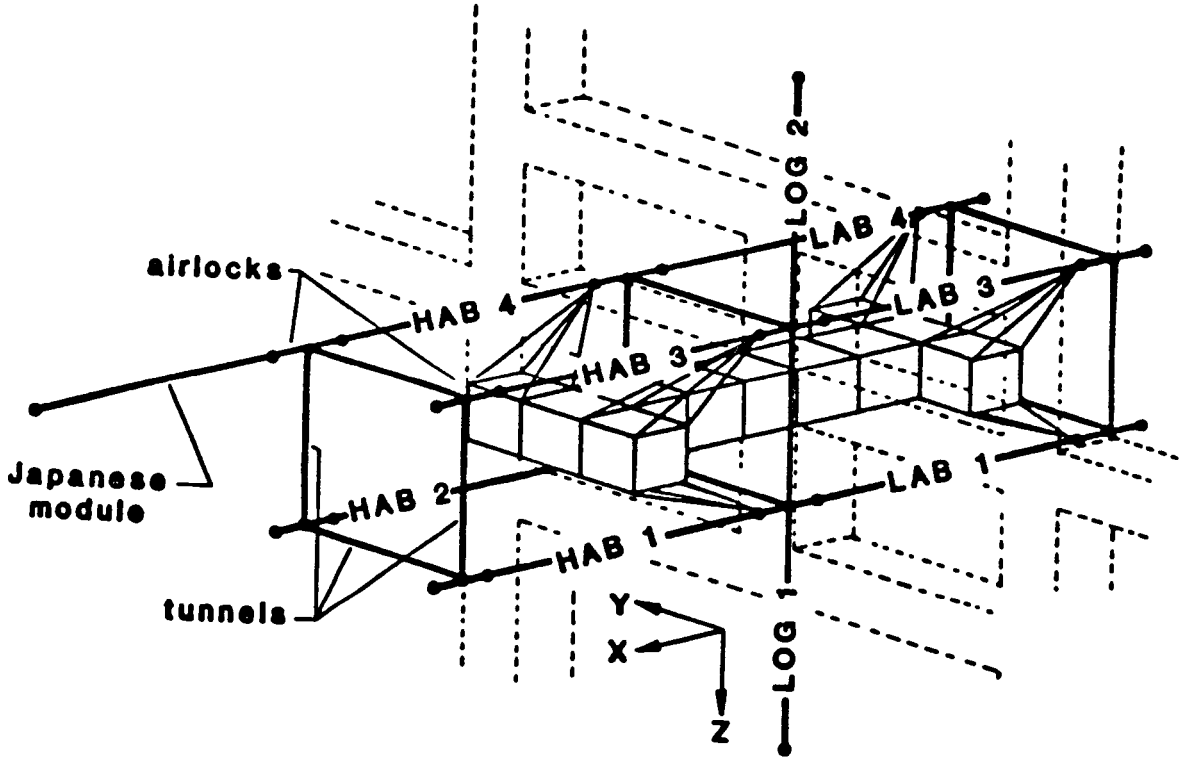

Figure 2b.- Sketch of module support truss structure.

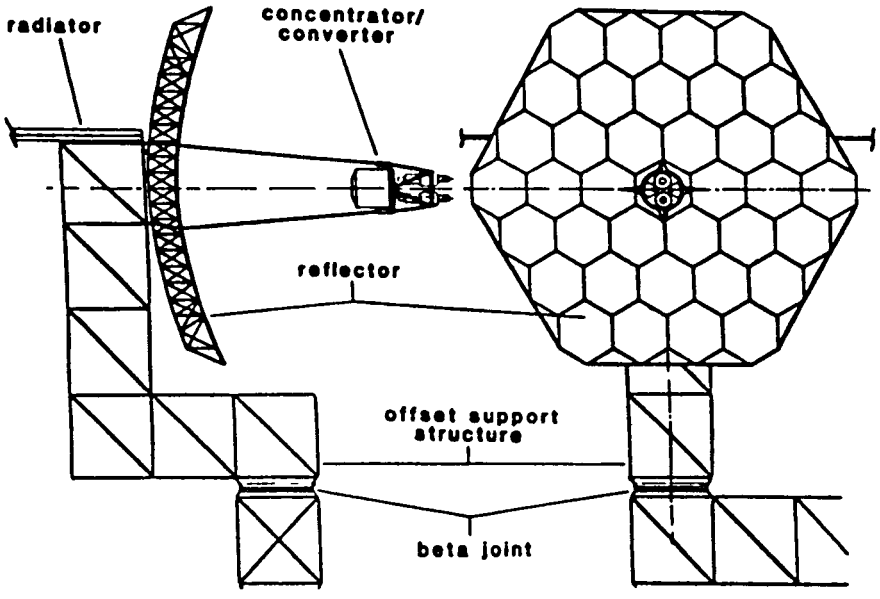

Figure 3a.- Sketch of typical solar dynamic unit.

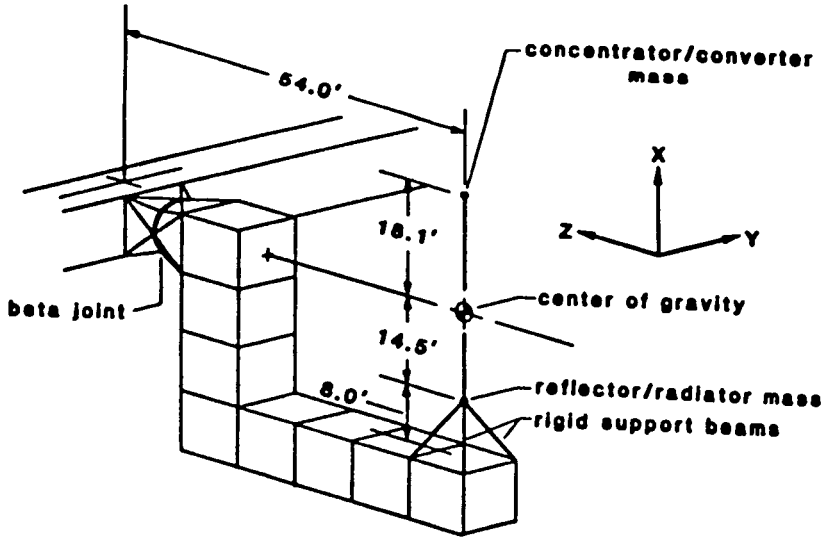

Figure 3b.- Approximation of mass distribution of solar dynamic unit and superstructure.

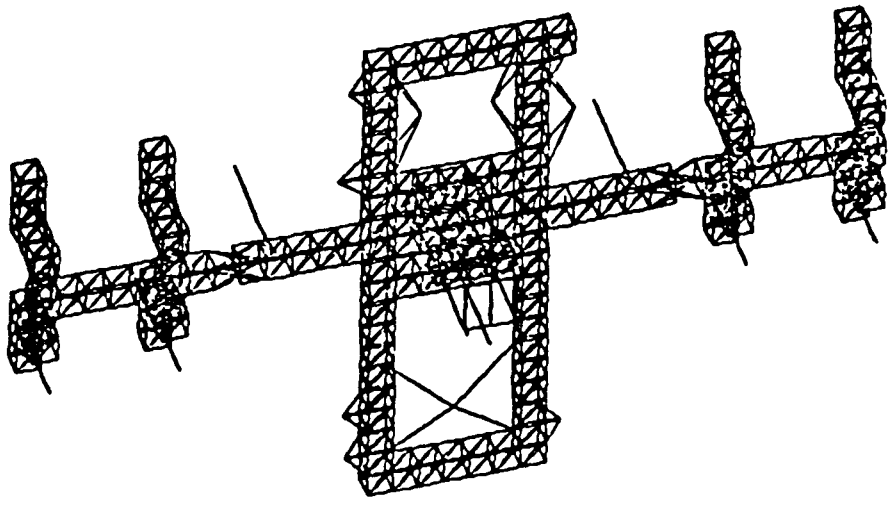

Figure 4a.- Finite Element model of the 5-meter bay space station.

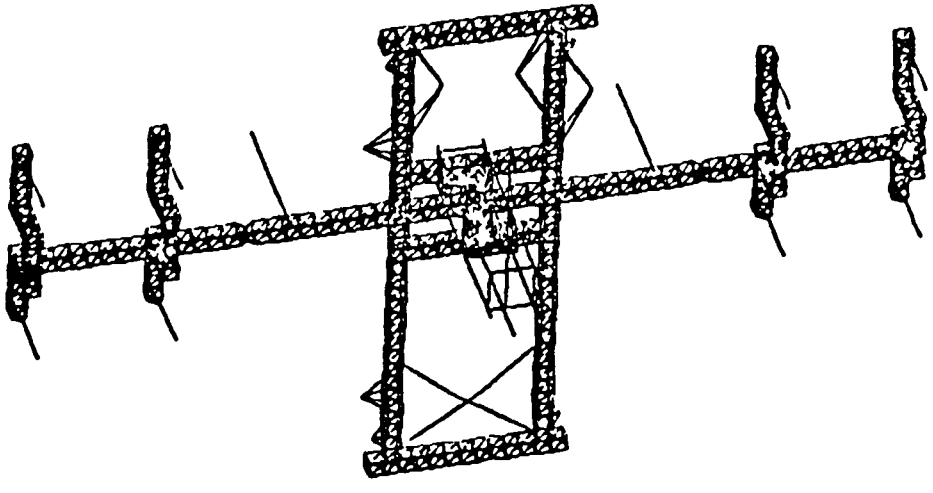

Figure 4b.- Finite Element model of the 9-foot bay space station.

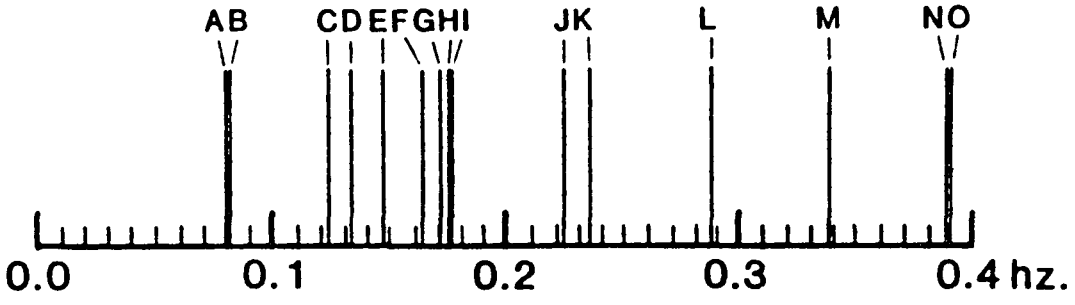

(a) 5-meter.

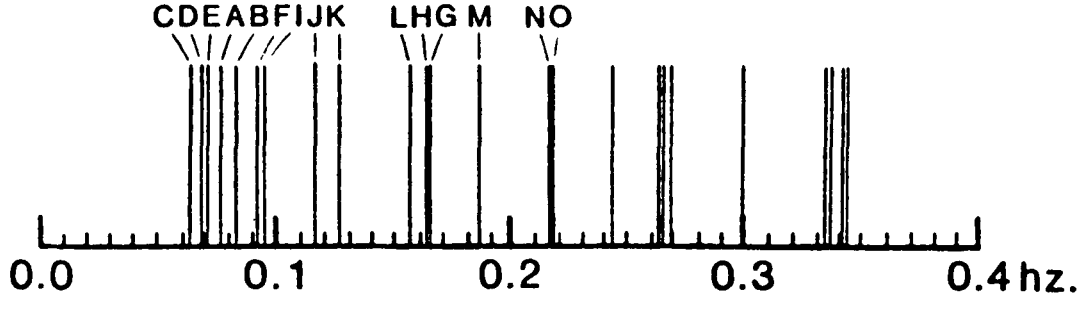

(b) 9-foot.

Figure 5.- Comparison of frequencies and mode shapes for two configurations.

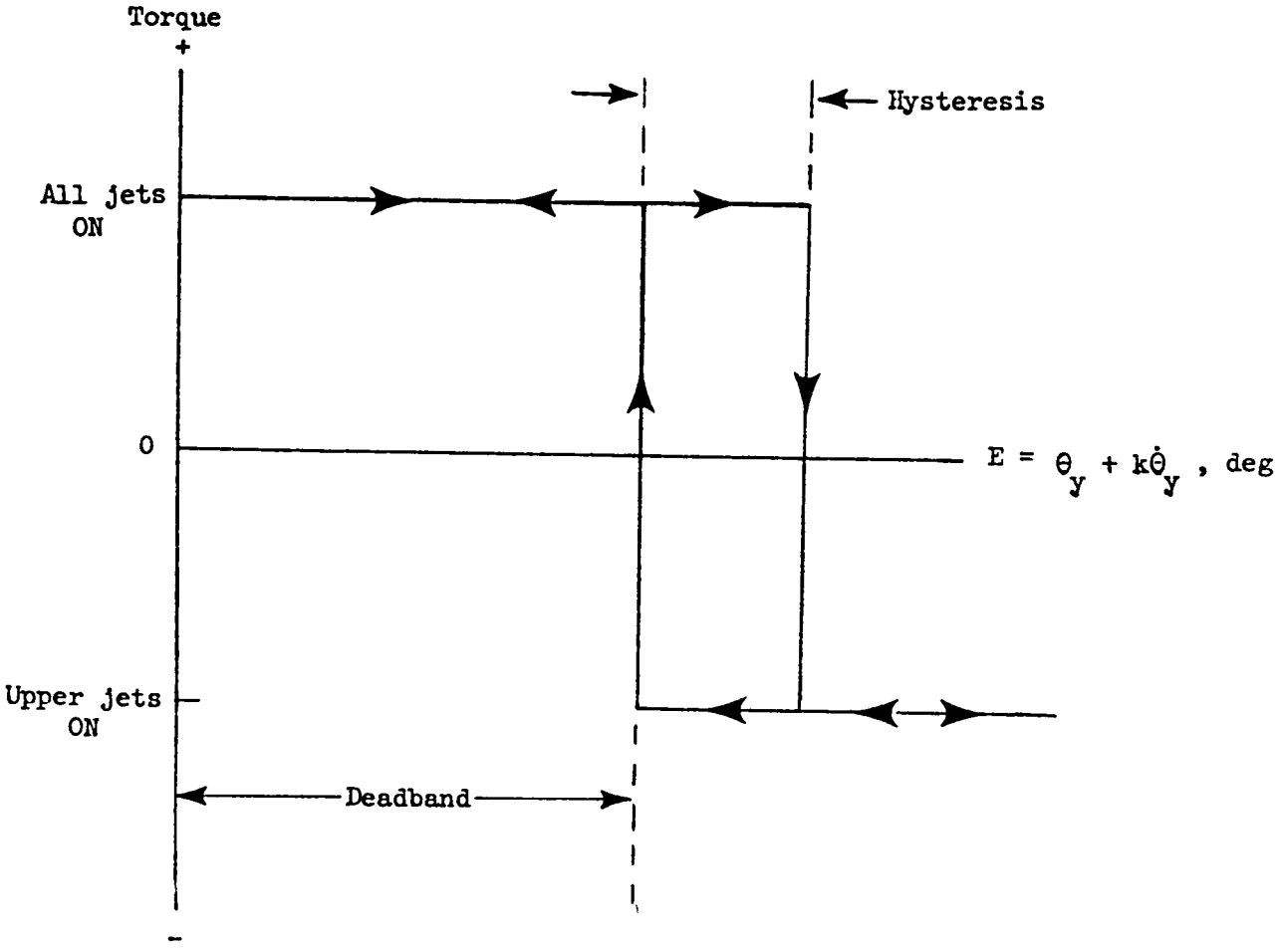

Figure 6.- Reboost control switching logic.
(Deadband = 1°, Hysteresis = $.05^{\circ}$, k = 1 sec.)

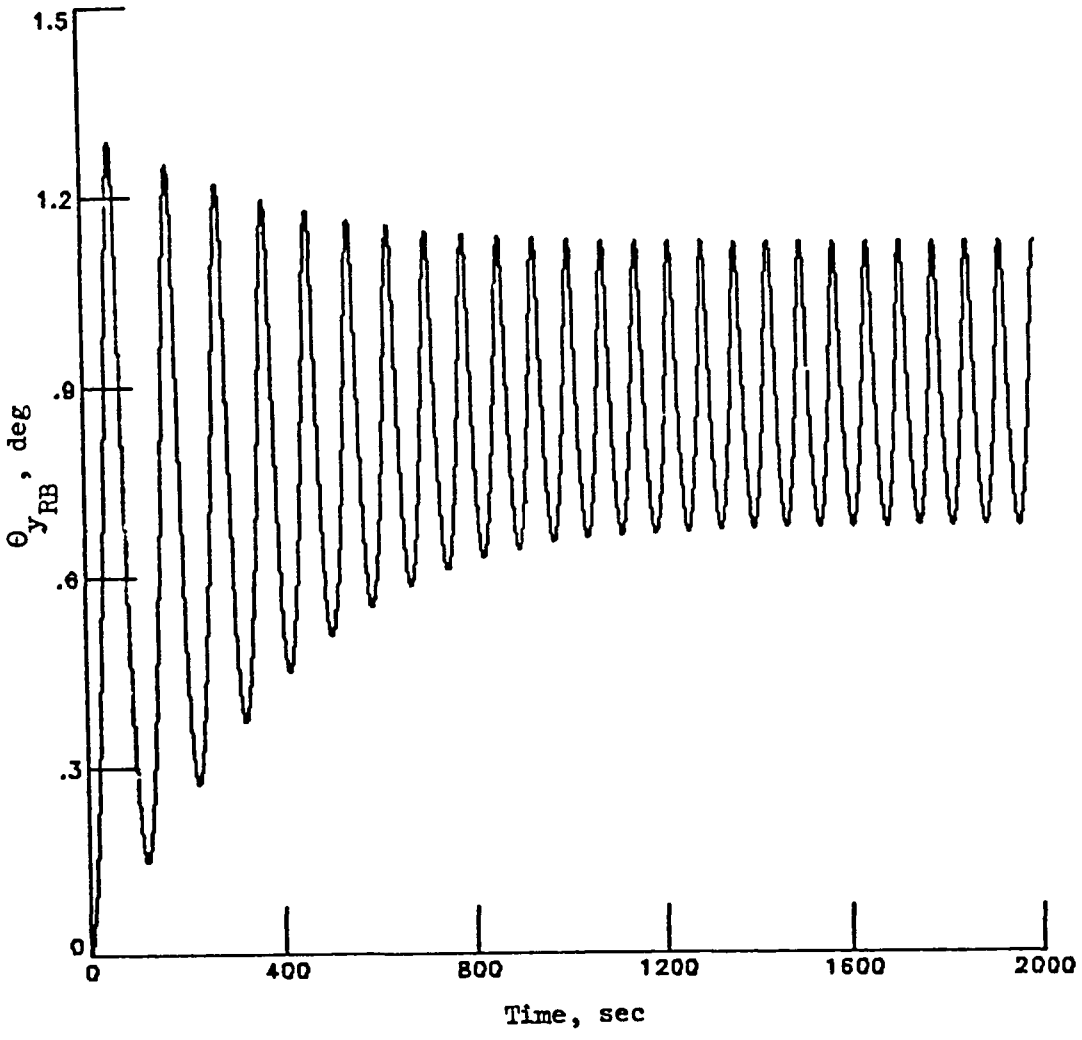

(a) Pitch angle.

Figure 7.- Typical rigid body response during reboost maneuver for 9-foot station.

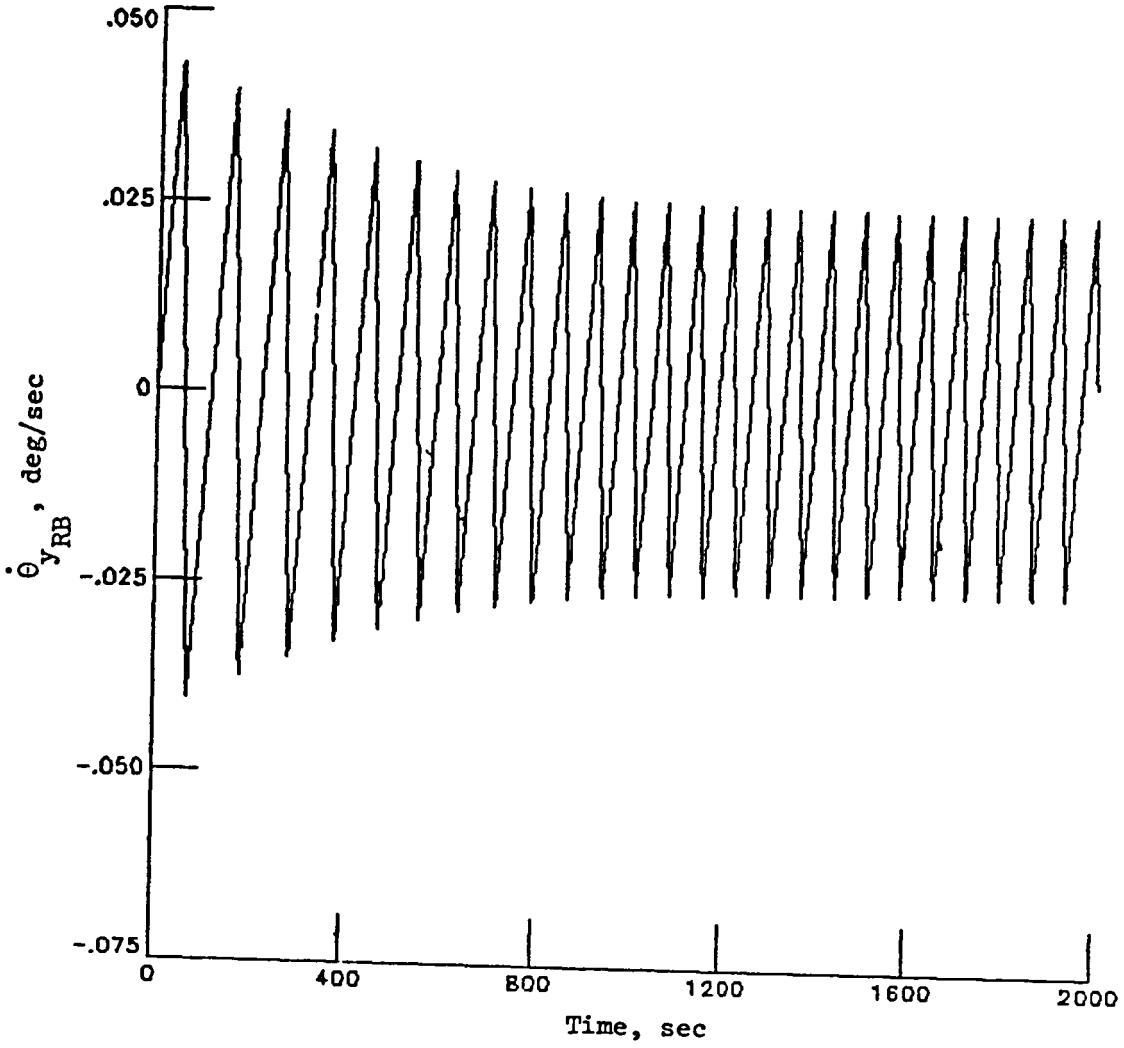

(b) Pitch rate.

Figure 7.- Continued.

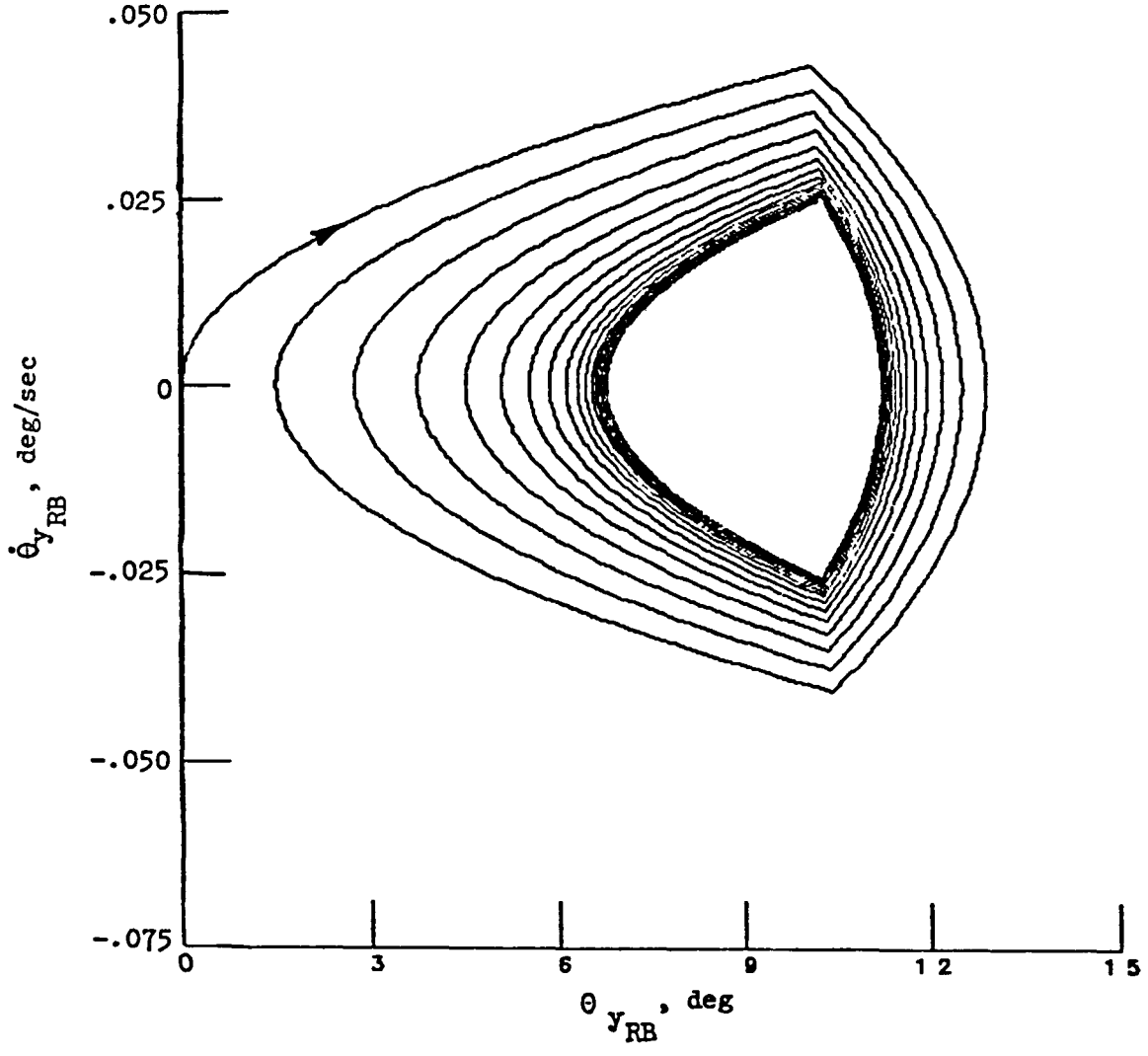

(c) Phase plane.

Figure 7.- Continued.

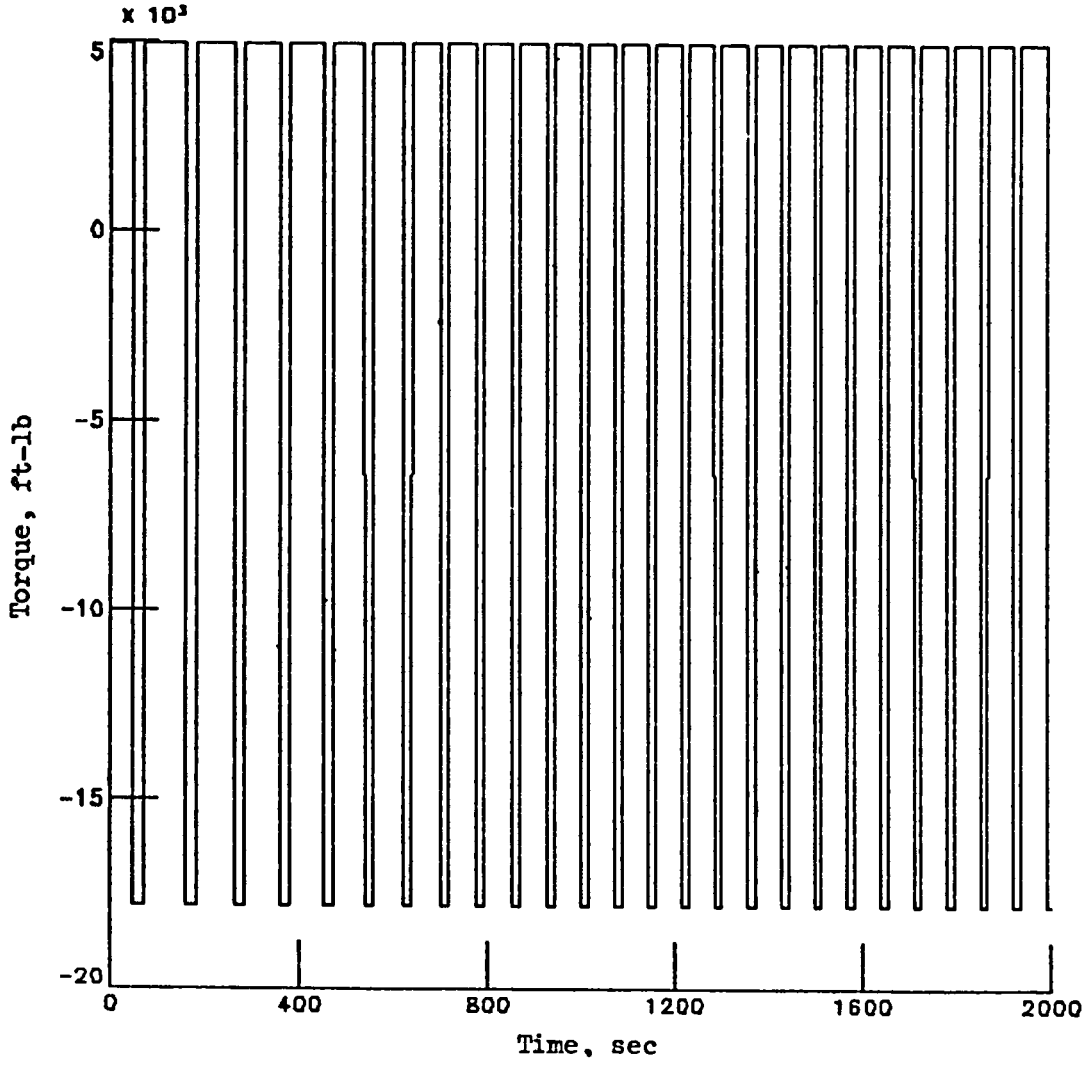

(d) Y-axis torque about center of gravity.

Figure 7.- Concluded.

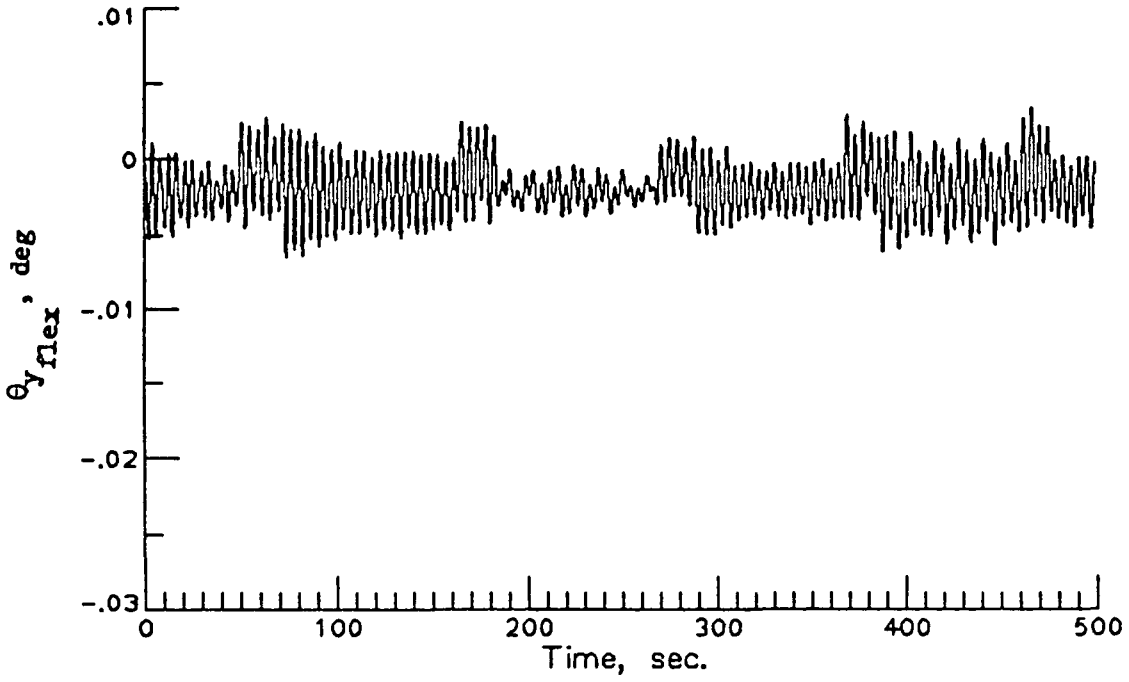

(a) 5-meter.

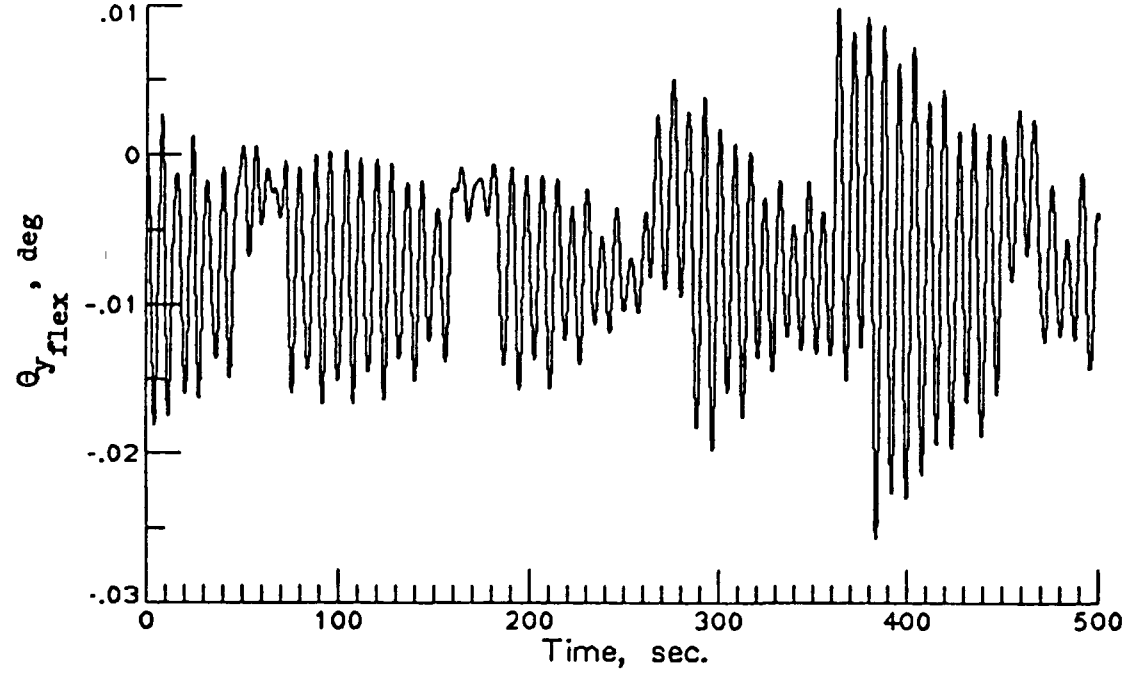

(b) 9-foot.

Figure 8.- Flexible contribution to pitch angle at sensor location during reboost maneuver.

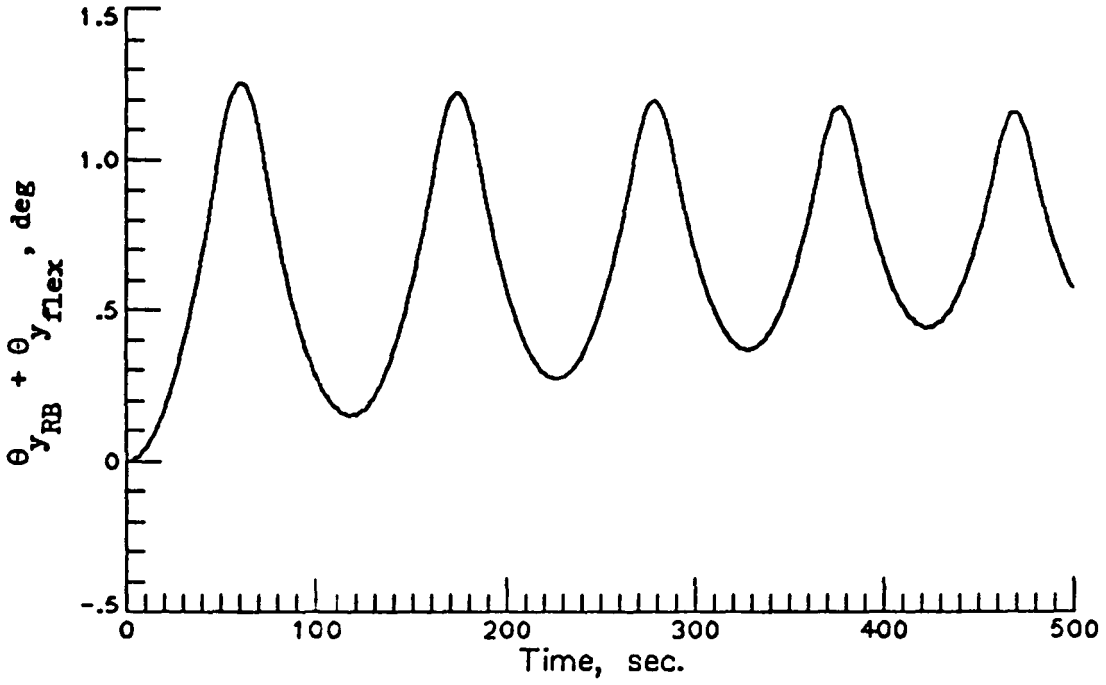

(a) 5-meter.

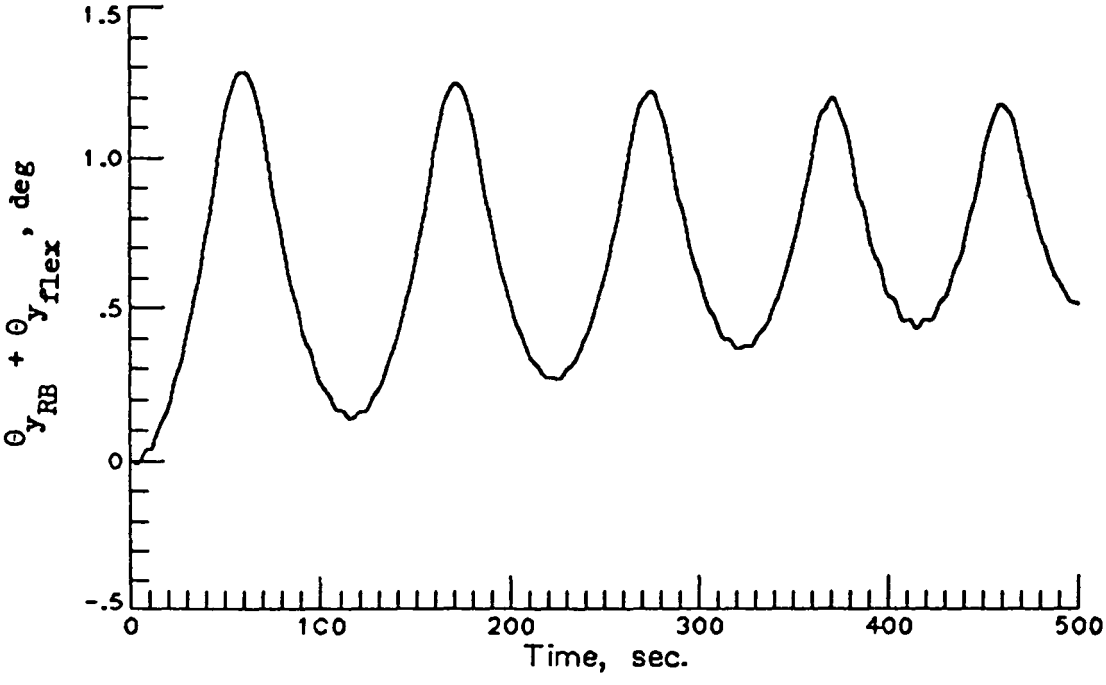

(b) 9-foot.

Figure 9.- Total pitch angle at sensor location during reboost maneuver.

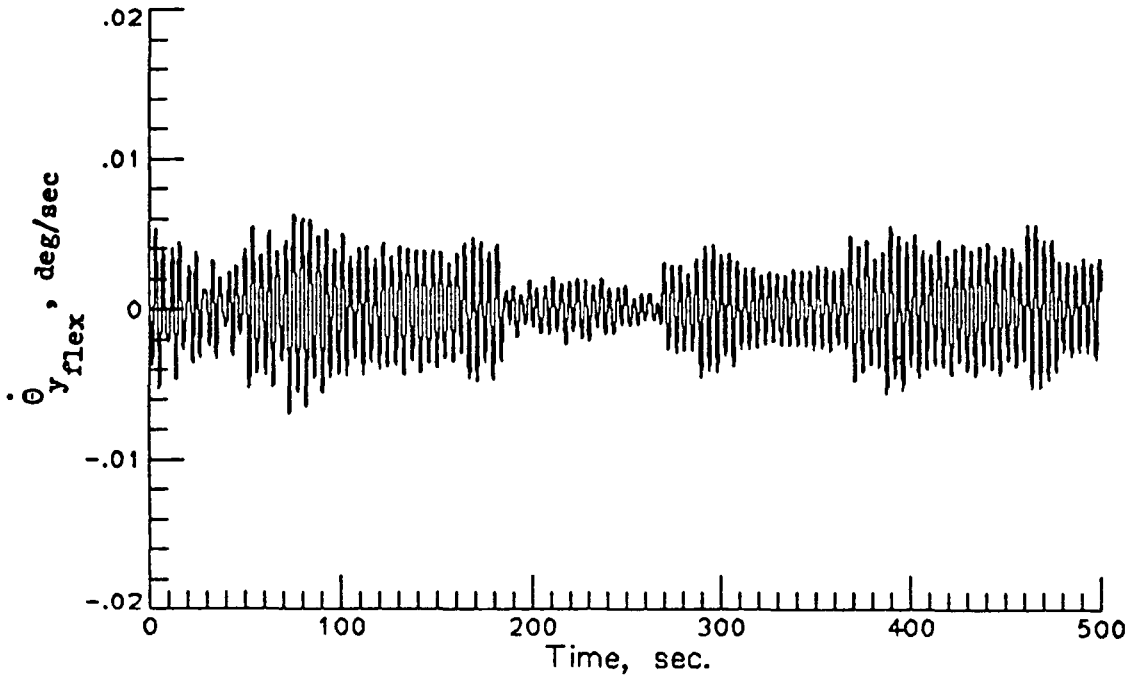

(a) 5-meter.

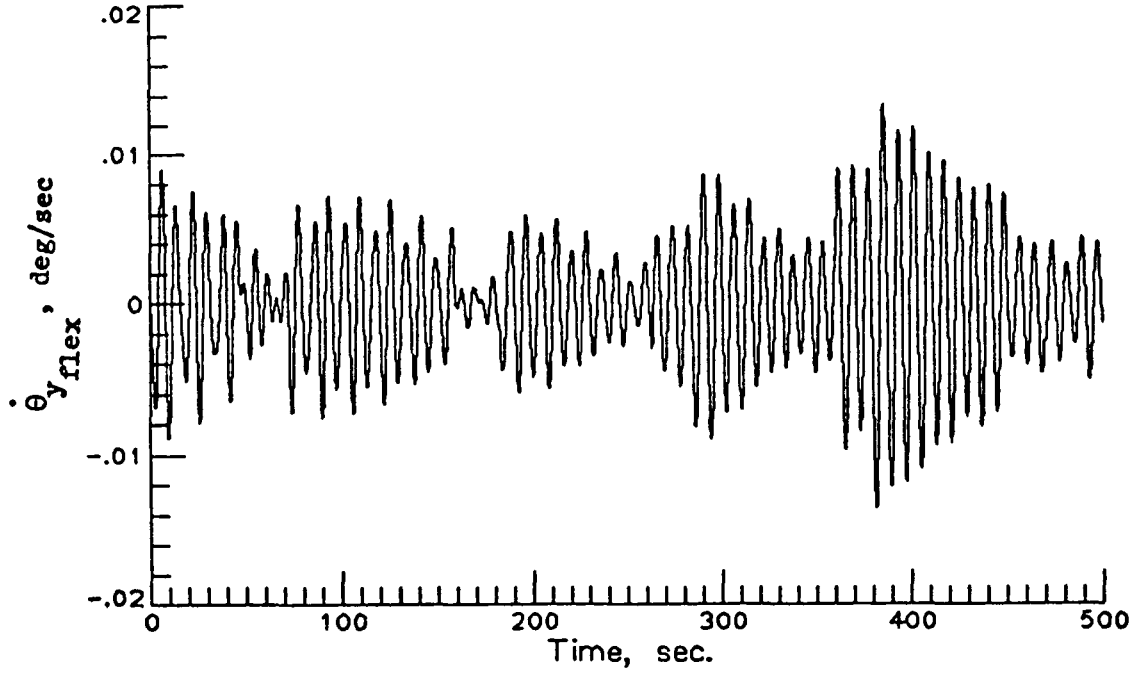

(b) 9-foot.

Figure 10.- Flexible contribution to pitch rate at sensor location during reboost maneuver.

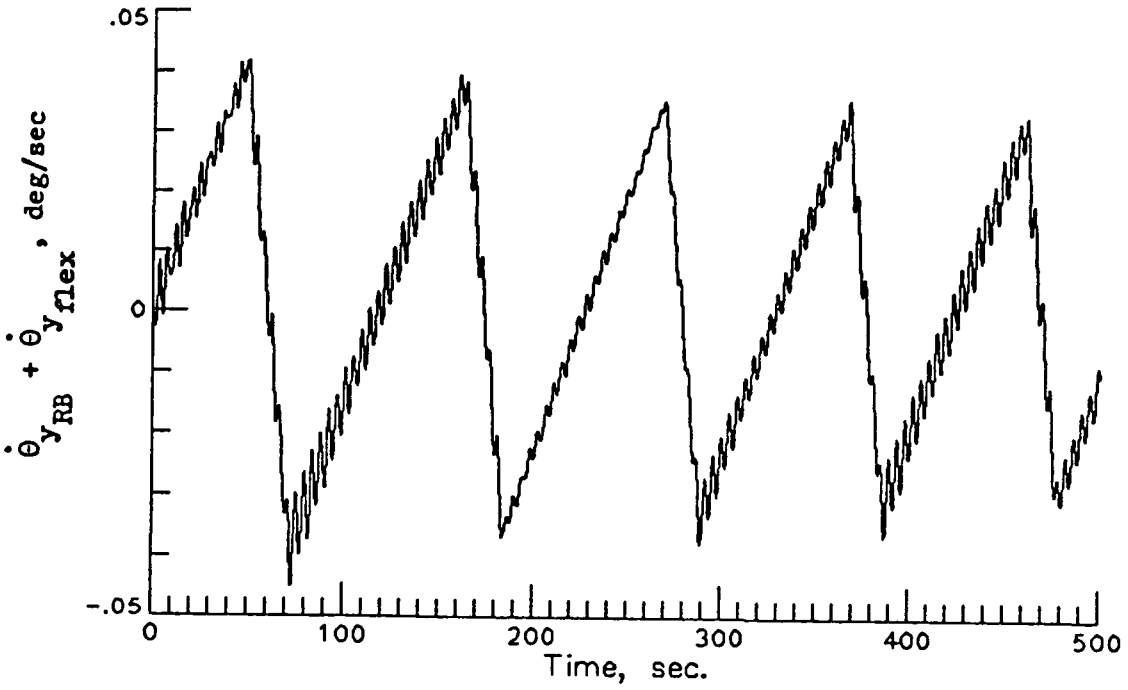

(a) 5-meter.

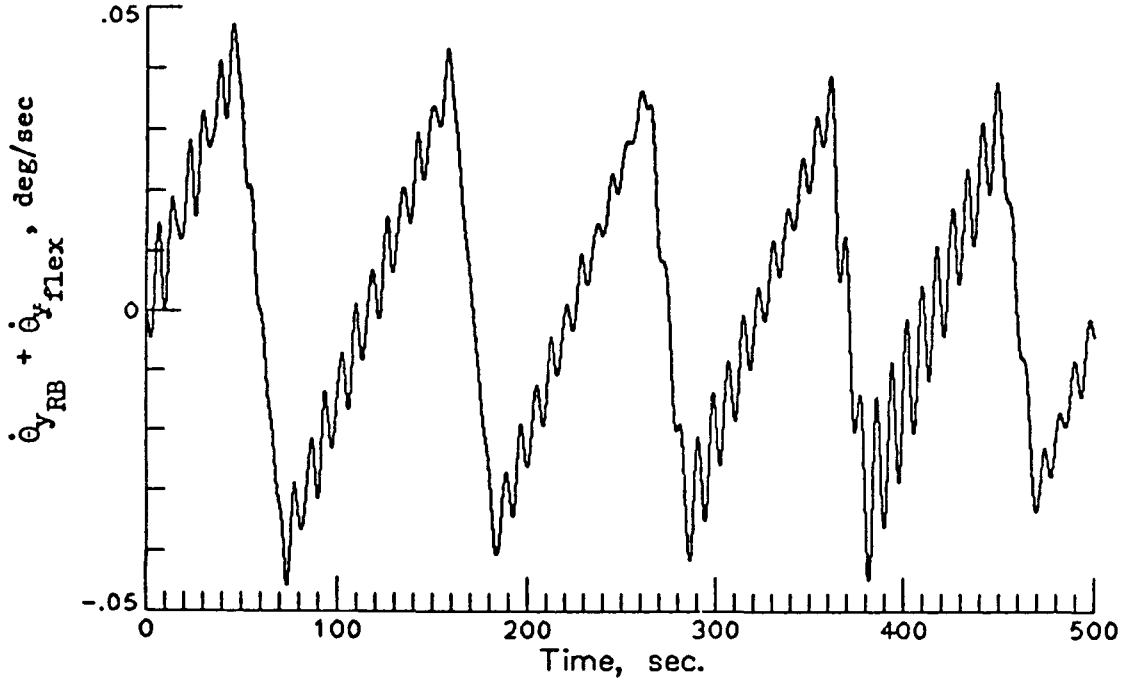

(b) 9-foot.

Figure 11.- Total pitch rate at sensor location during reboost maneuver.

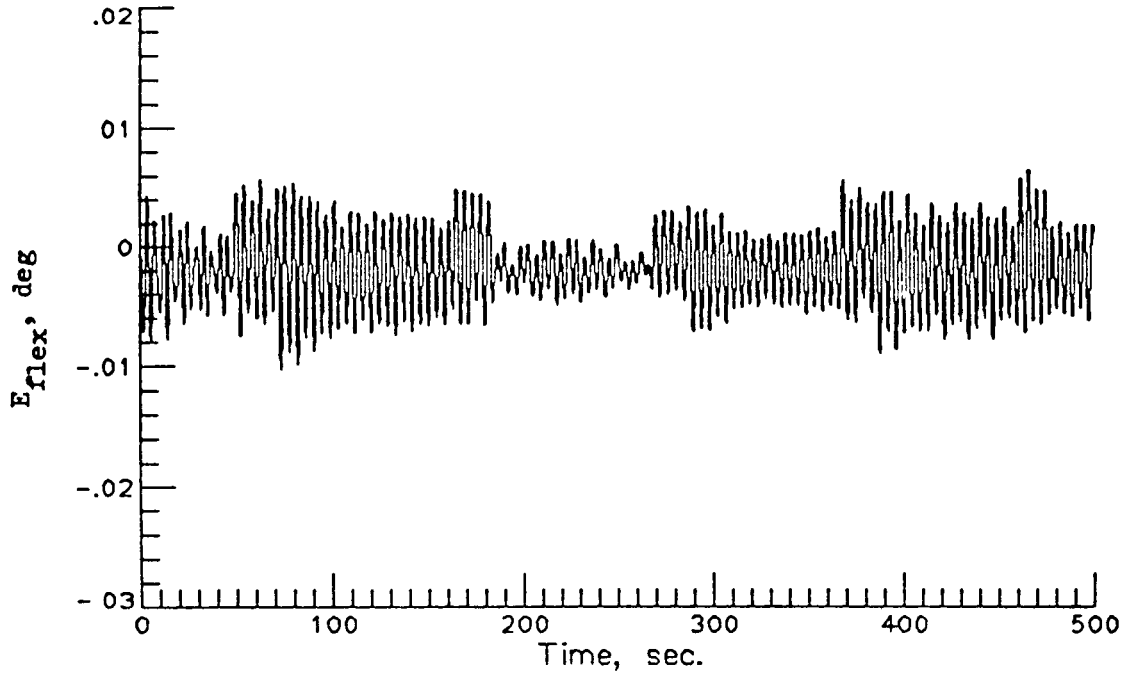

(a) 5-meter.

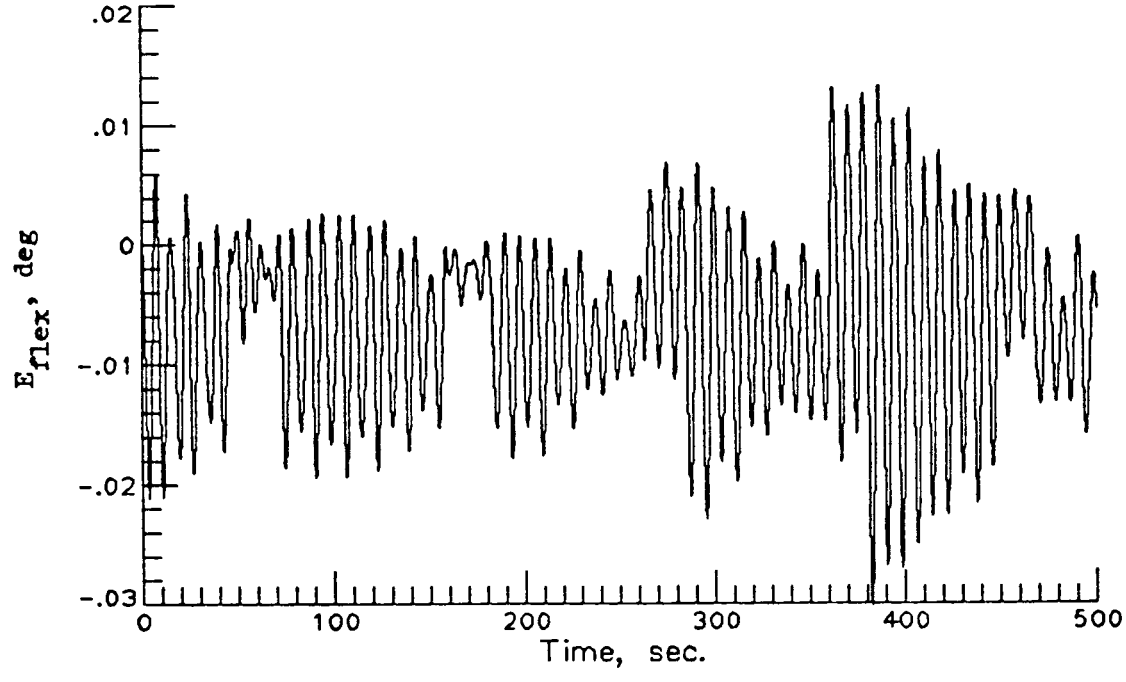

(b) 9-foot.

Figure 12.- Flexible contribution to error signal at sensor location during reboost maneuver. ($E_{flex} = \theta_{y_{flex}} + k\dot{\theta}_{y_{flex}}$.)

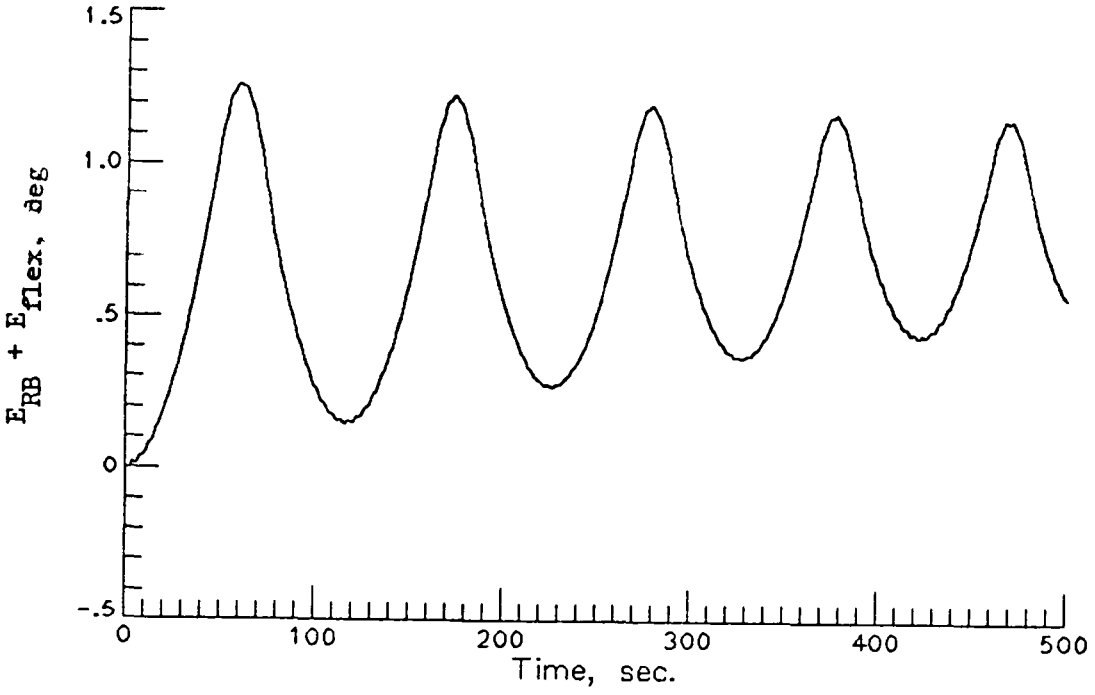

(a) 5-meter.

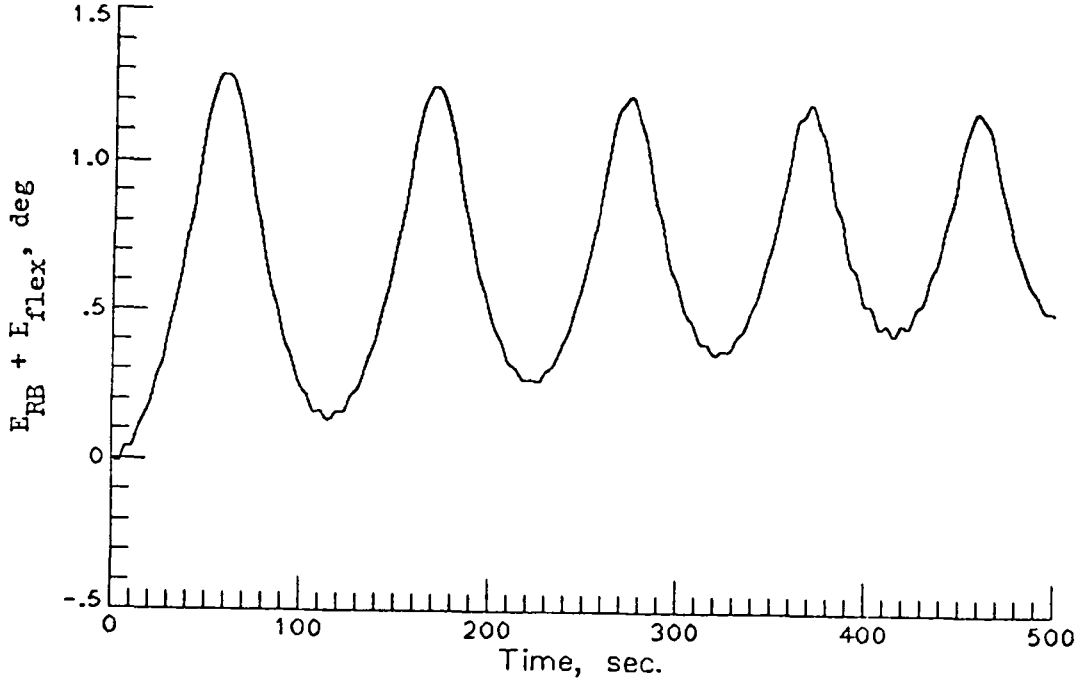

(b) 9-foot.

Figure 13.- Total error signal at sensor location during reboost maneuver. ($E_{RB} = \theta_{y_{RB}} + k\dot{\theta}_{y_{RB}}$.)

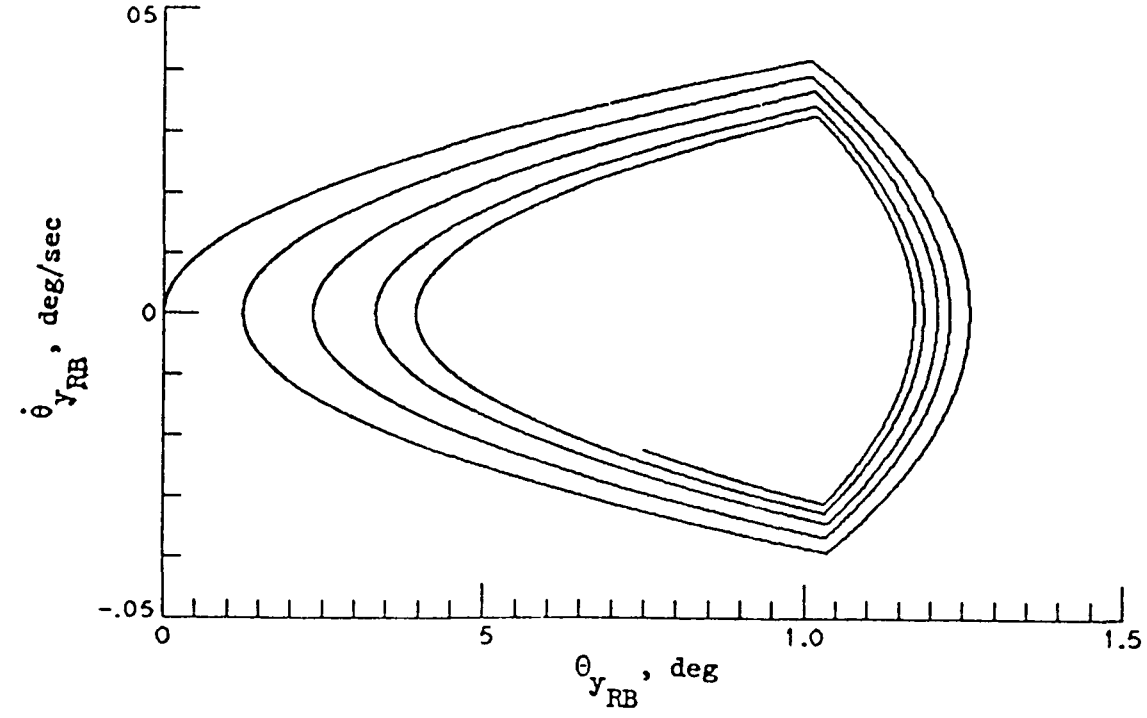

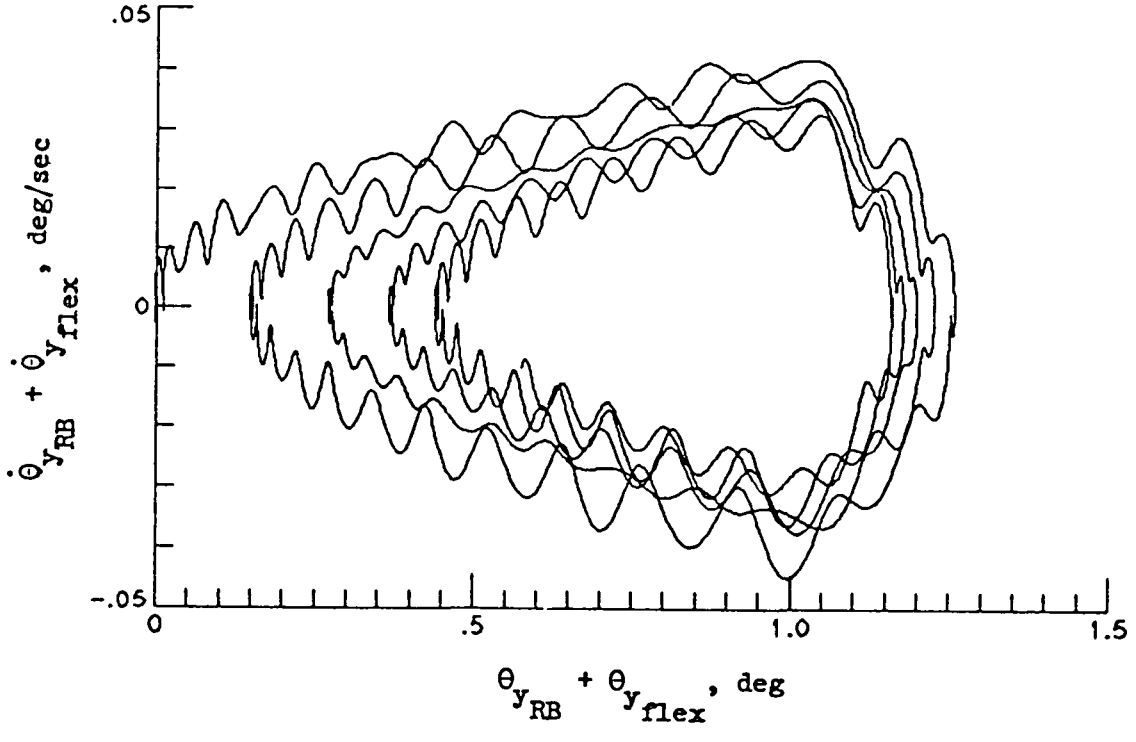

(a) 5-meter.

Figure 14.- Phase plane representation of reboost maneuver.

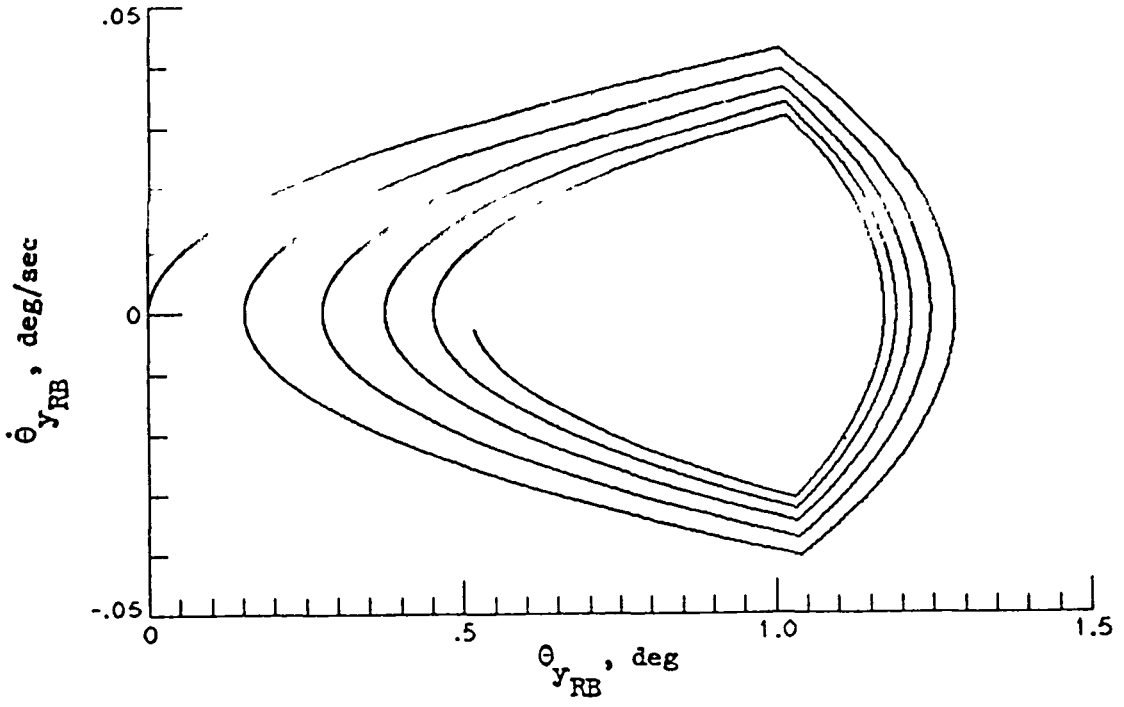

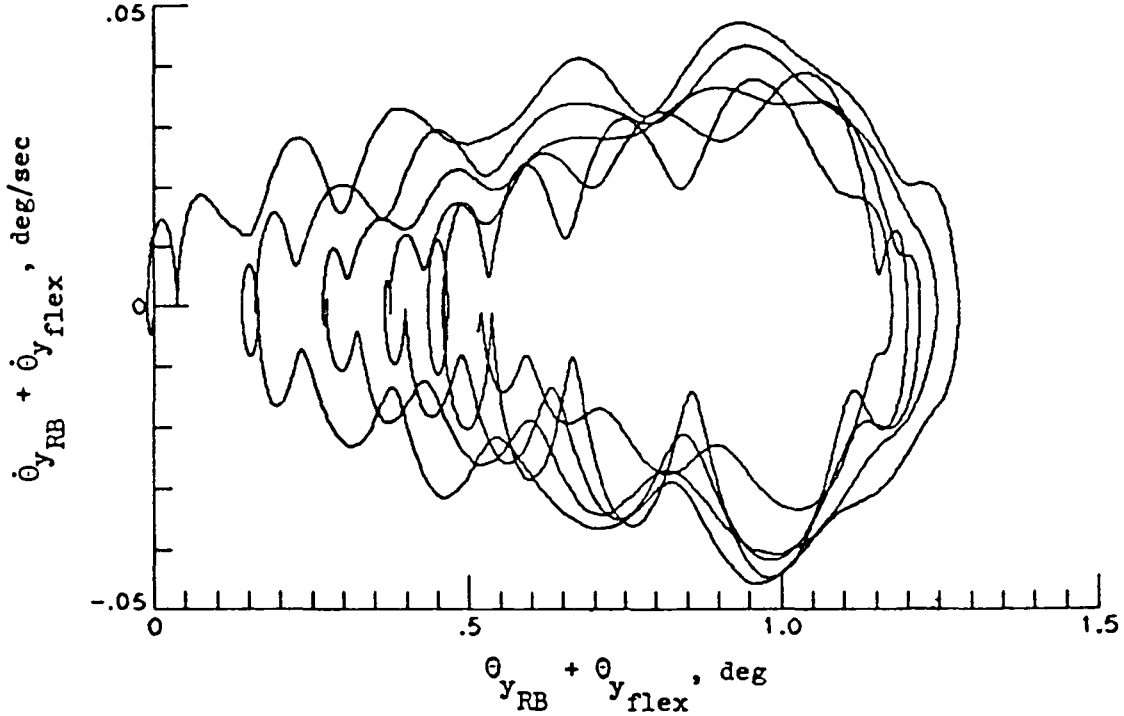

(b) 9-foot.

Figure 14.- Concluded.

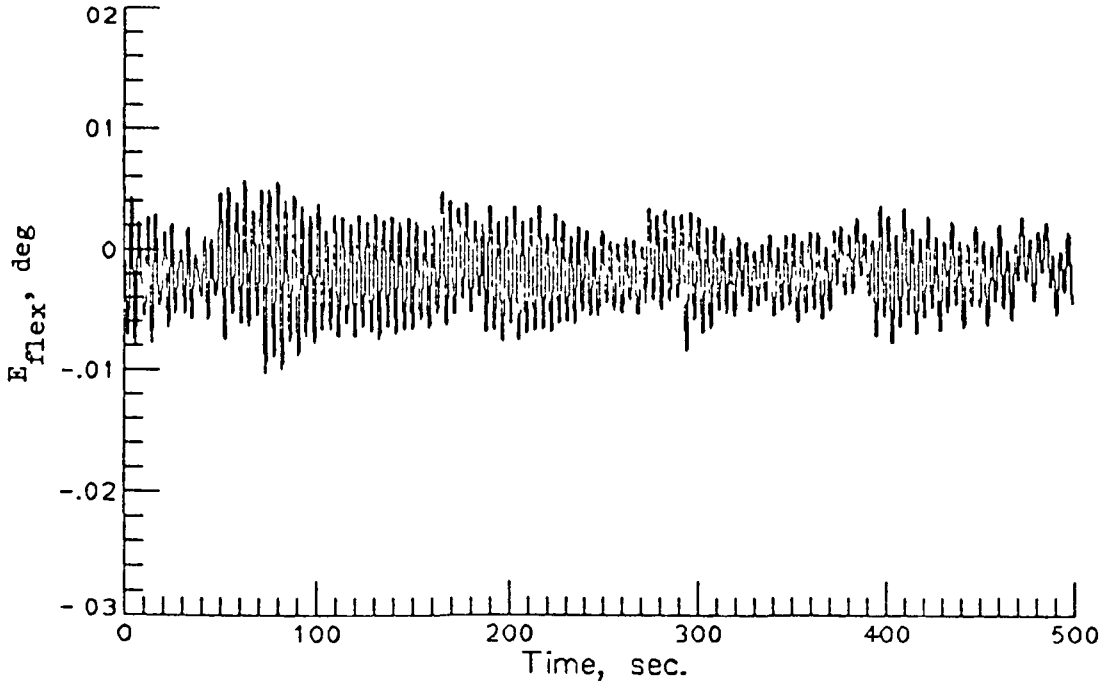

(a) 5-meter.

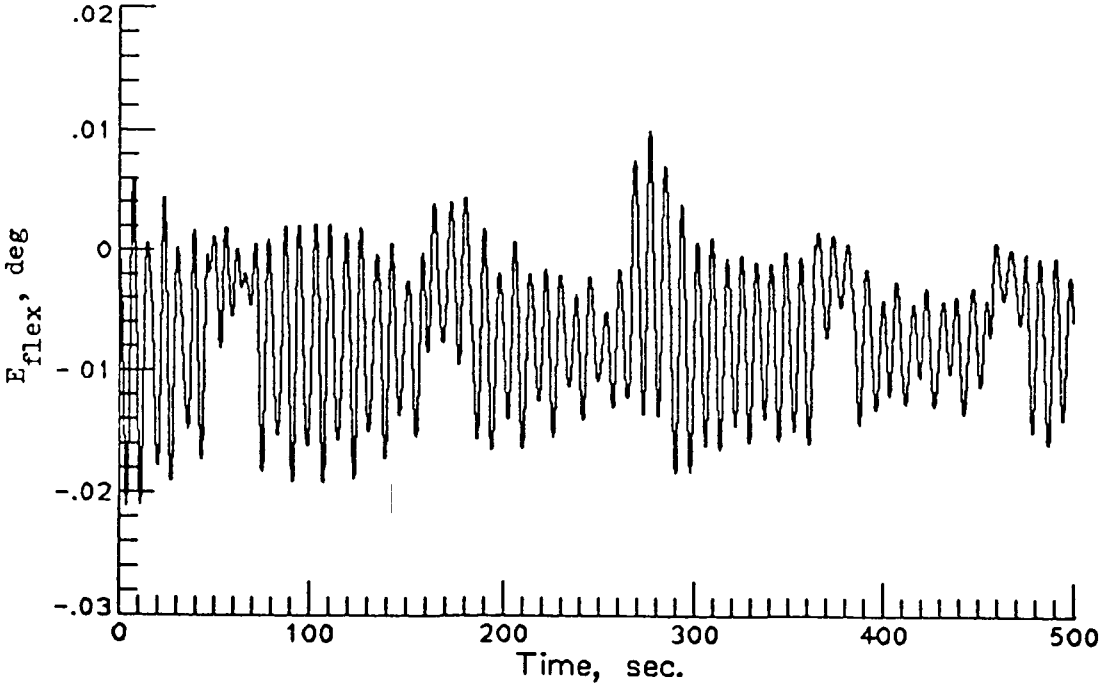

(b) 9-foot.

Figure 15.- Flexible contribution to error signal using sensor output for control.

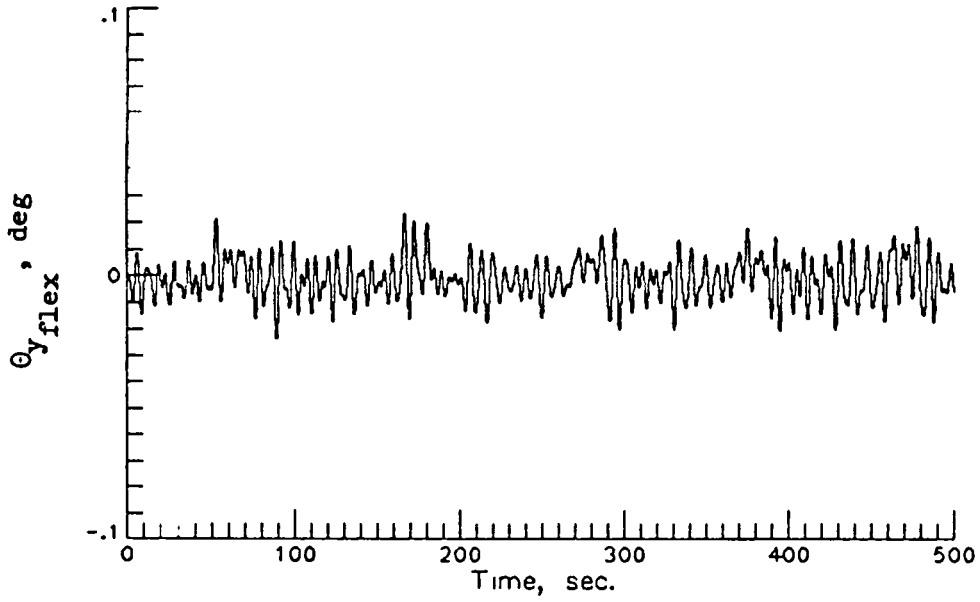

(a) 5-meter.

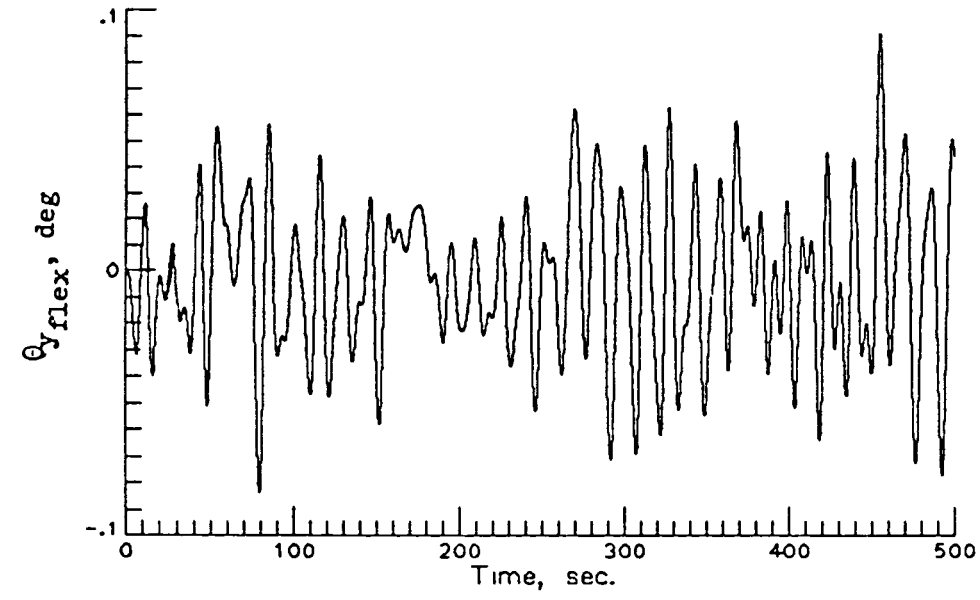

(b) 9-foot.

Figure 16.- Flexible contribution to Y-axis pitch angle at the outer solar collector during reboost maneuver.

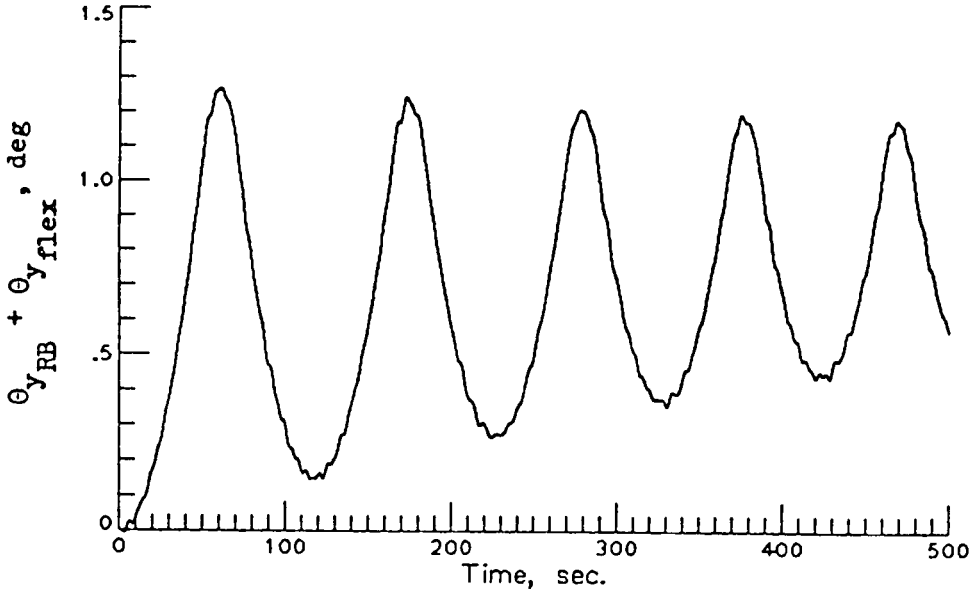

(a) 5-meter.

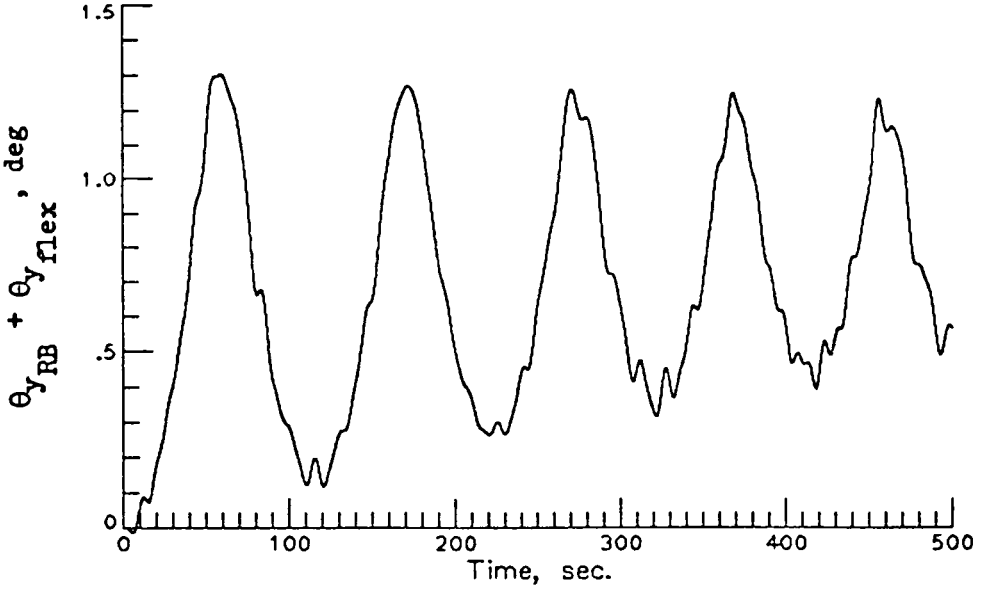

(b) 9-foot.

Figure 17.- Total Y-axis pitch angle at outer solar collector during reboost maneuver.

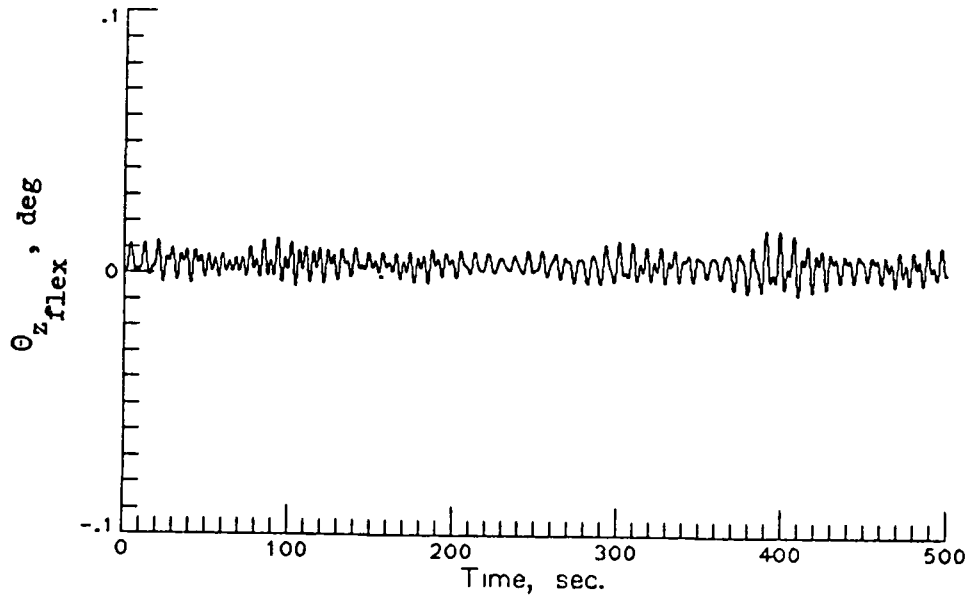

(a) 5-meter.

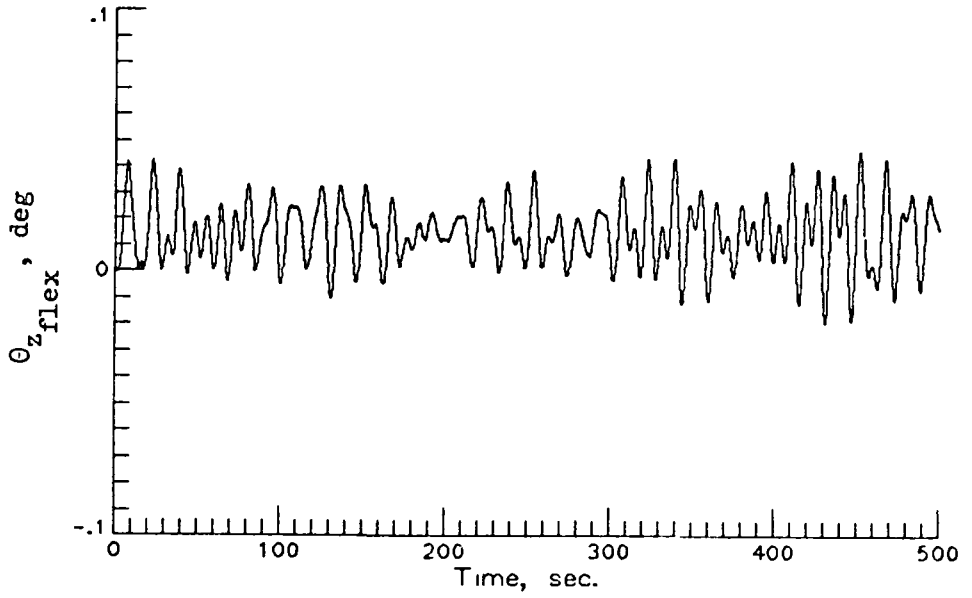

(b) 9-foot.

Figure 18.- Flexible contribution to Z-axis pitch angle at the outer solar collector during reboost maneuver.

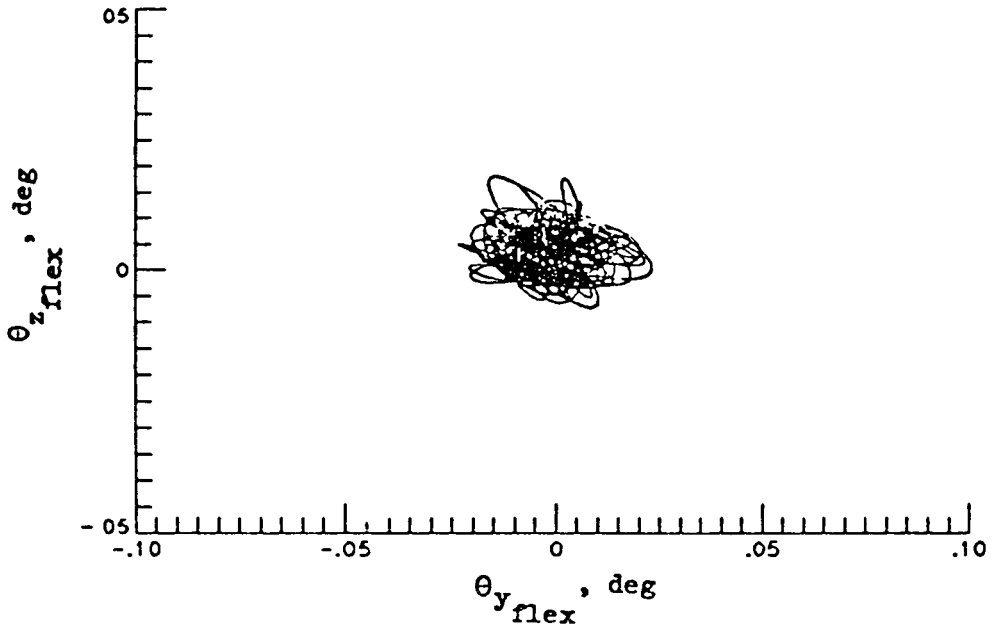

(a) 5-meter.

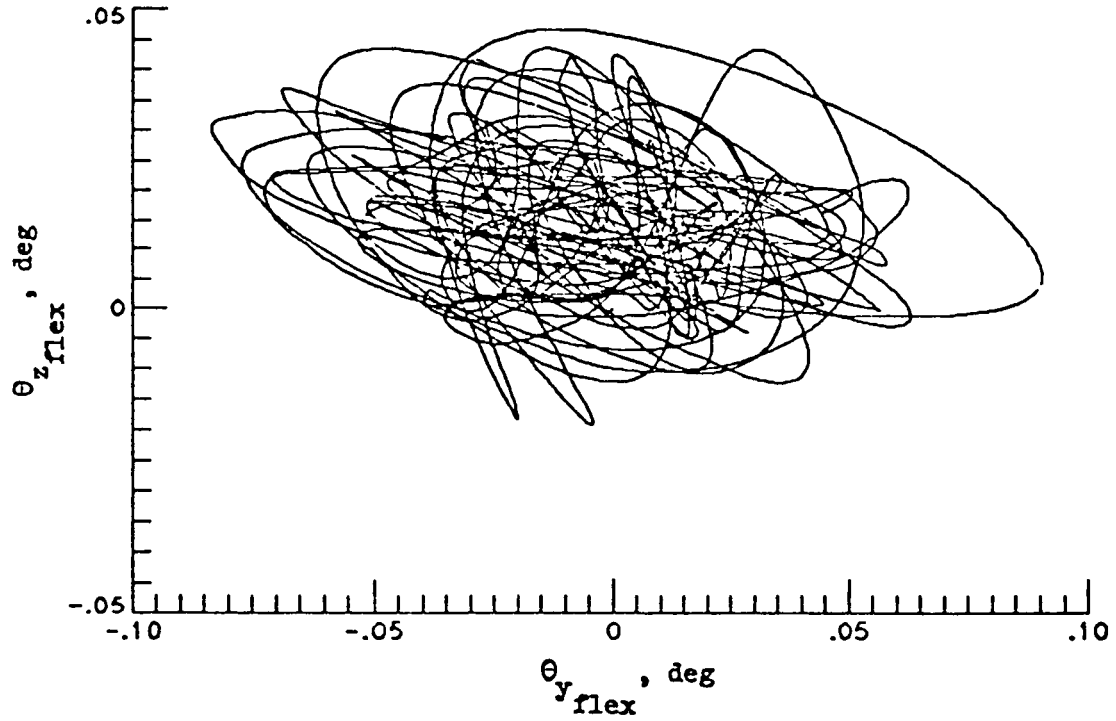

(b) 9-foot

Figure 19.- Flexible Sun line variations at outer solar collector during reboost maneuver.

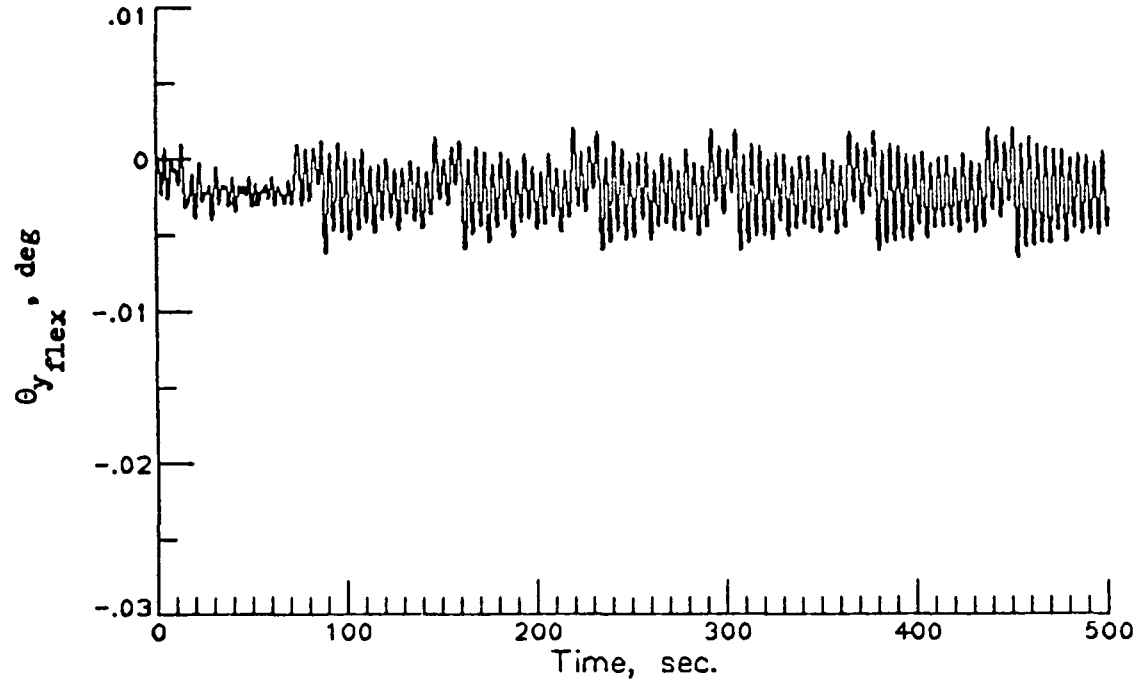

(a) Flexible pitch angle.

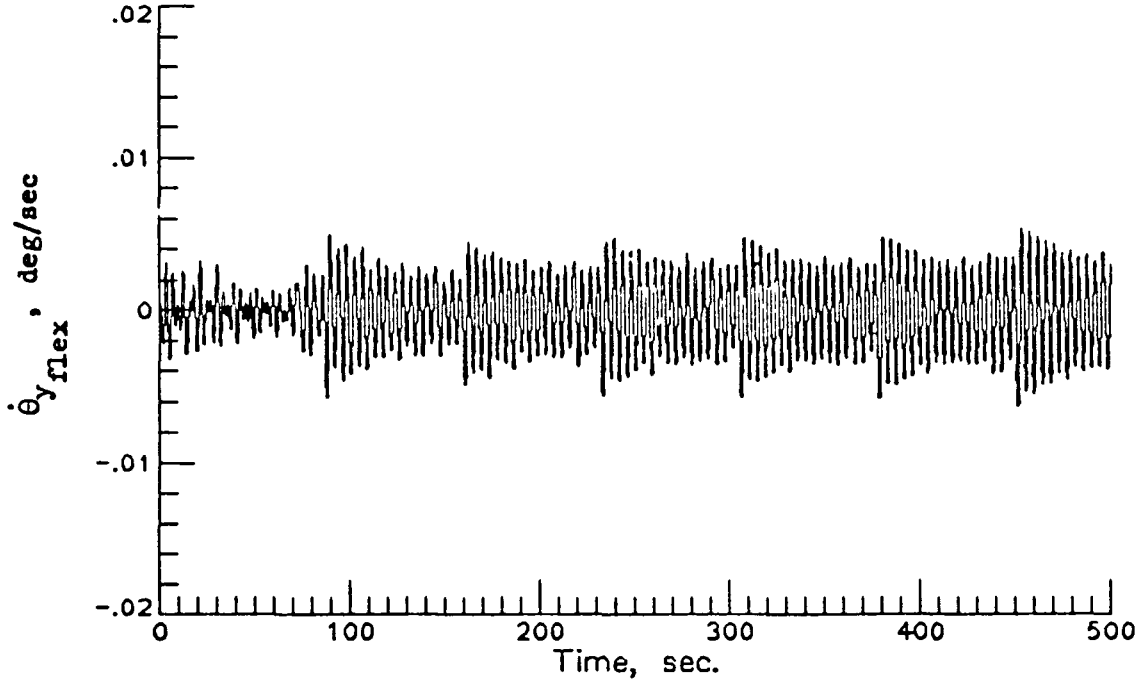

(b) Flexible pitch rate.

Figure 20.- Pitch and pitch rate variation at sensor location during reboost limit cycle. (5-meter)

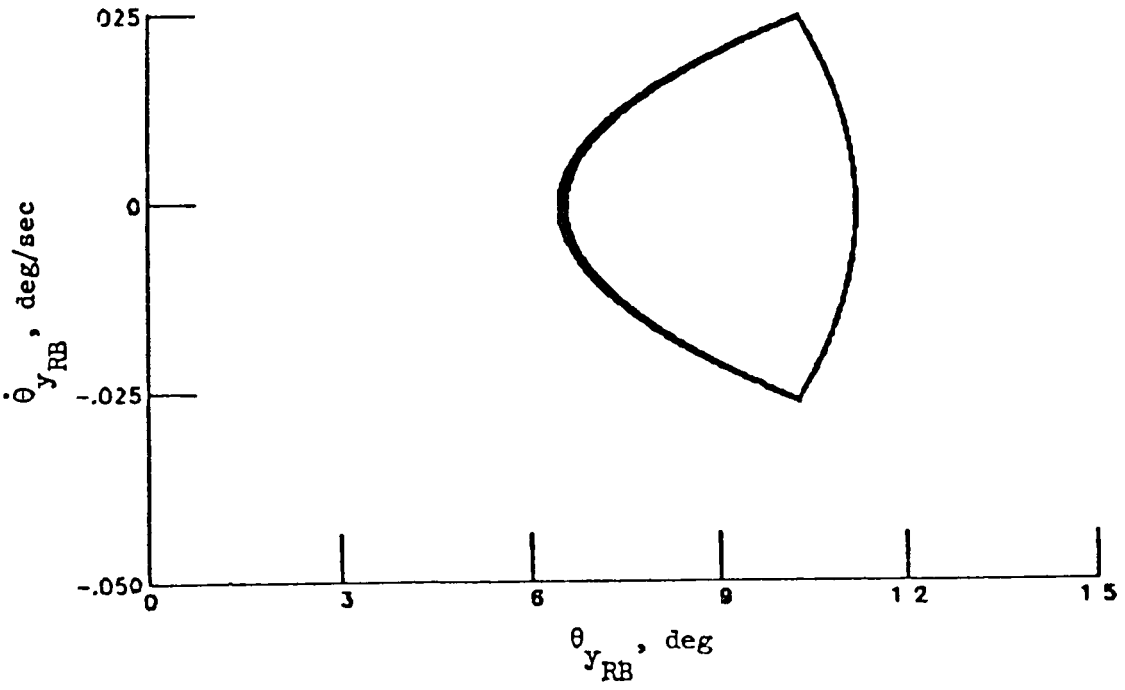

(c) Rigid body pitch, pitch rate phase plane representation.

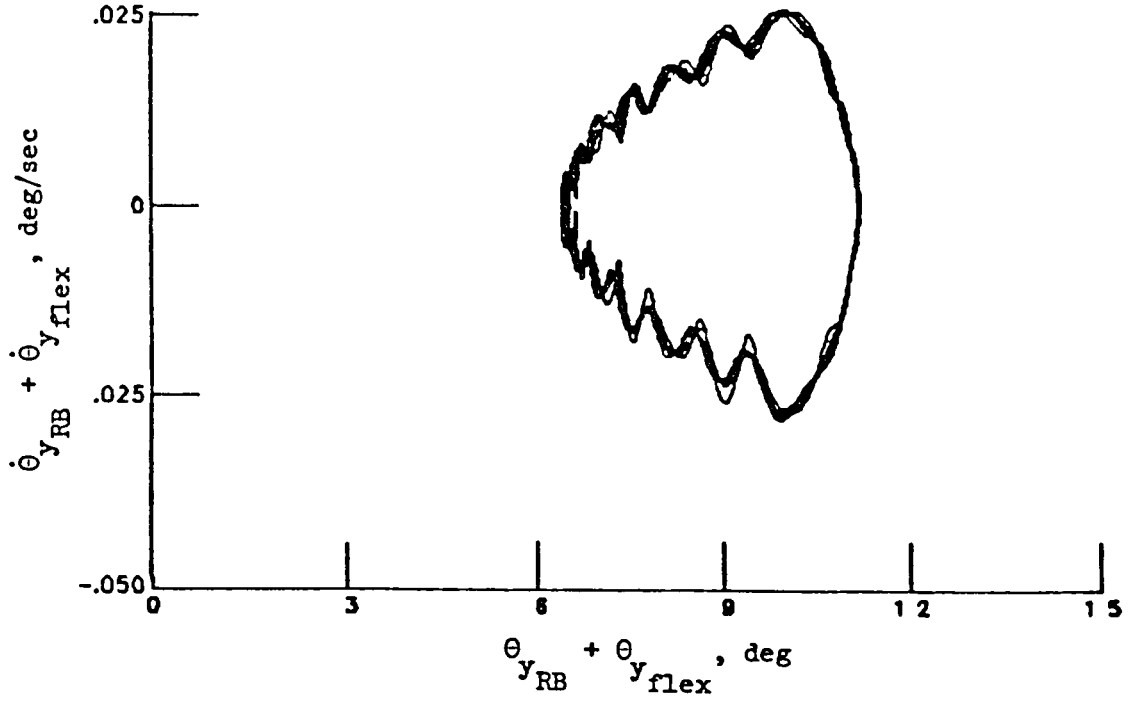

(d) Total pitch, pitch rate phase plane representation.

Figure 20.- Concluded.

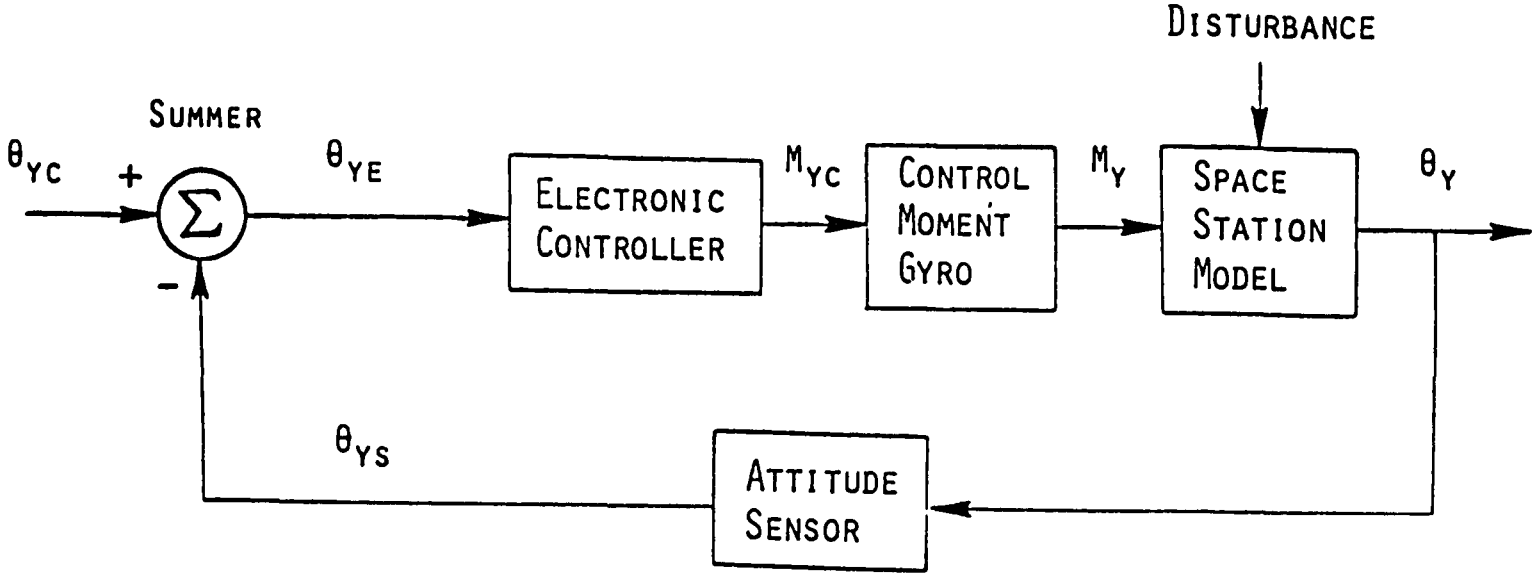

θ_Y - SPACE STATION ATTITUDE

θ_{YS} - SENSED ATTITUDE

θ_{YC} - COMMANDED ATTITUDE

θ_{YE} - ATTITUDE ERROR

M_Y - CONTROL MOMENT

M_{YC} - COMMANDED CONTROL MOMENT

Figure 21.- Block diagram of attitude control system.

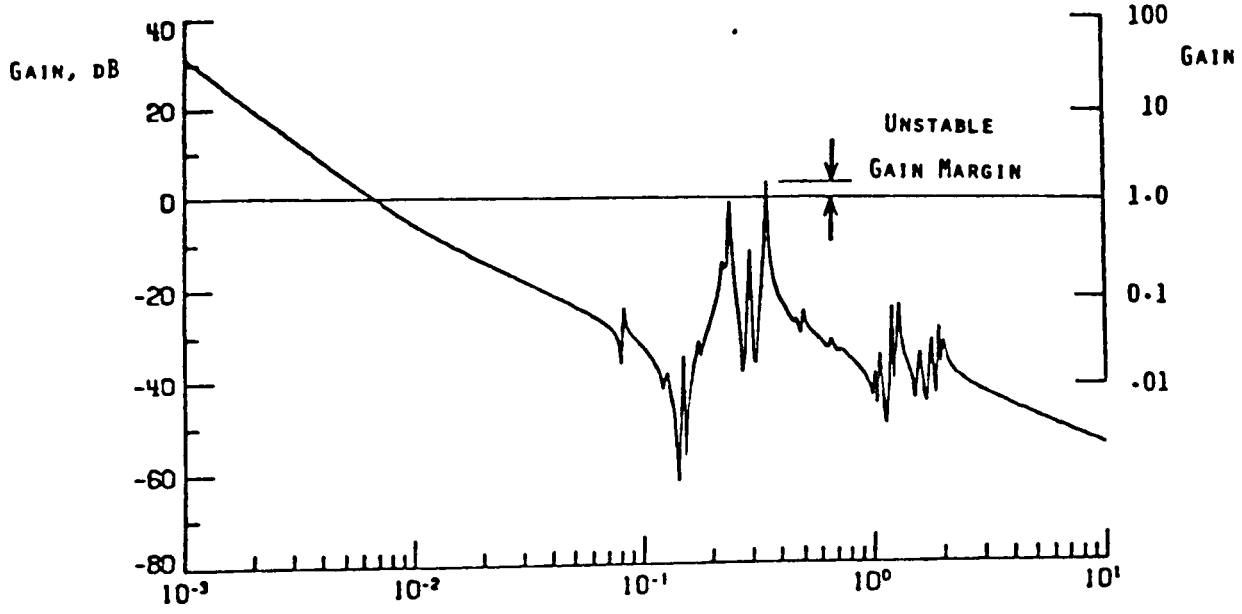

(a) Gain.

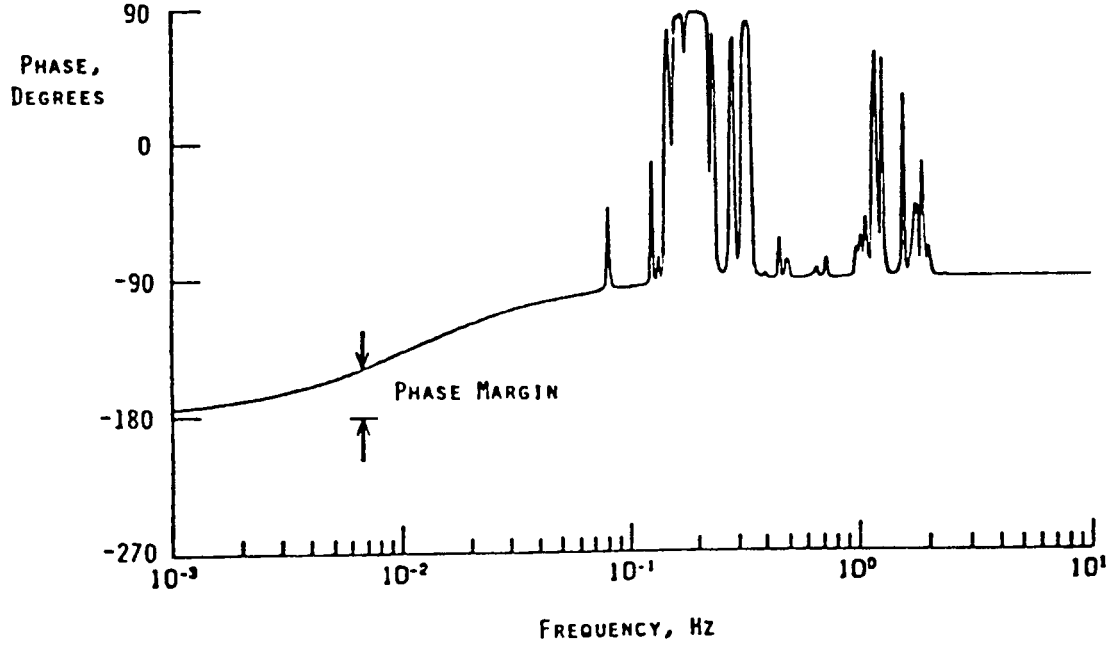

(b) Phase.

Figure 22.- Frequency response, 5-meter space station, PD controller.

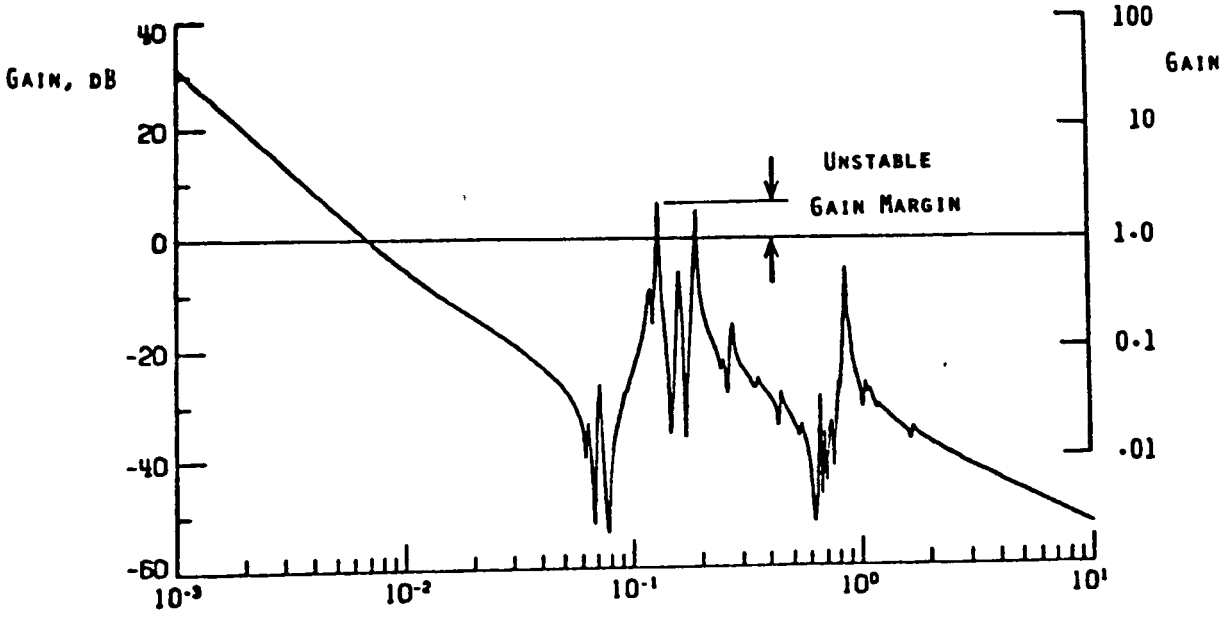

(a) Gain.

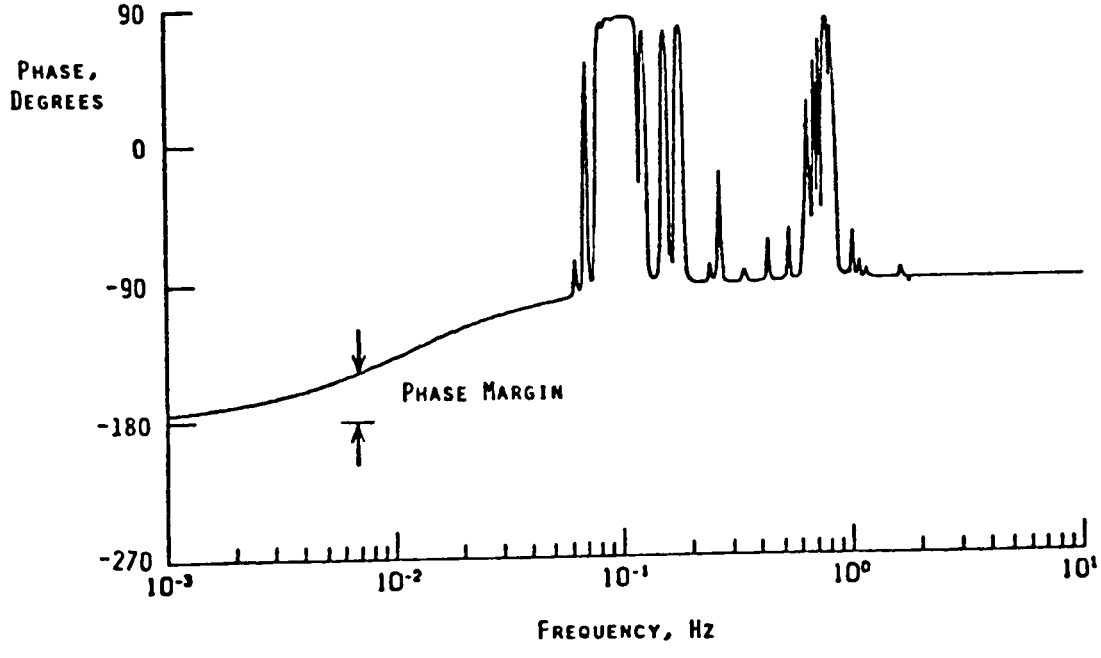

(b) Phase.

Figure 23.- Frequency response, 9-foot space station, PD controller.

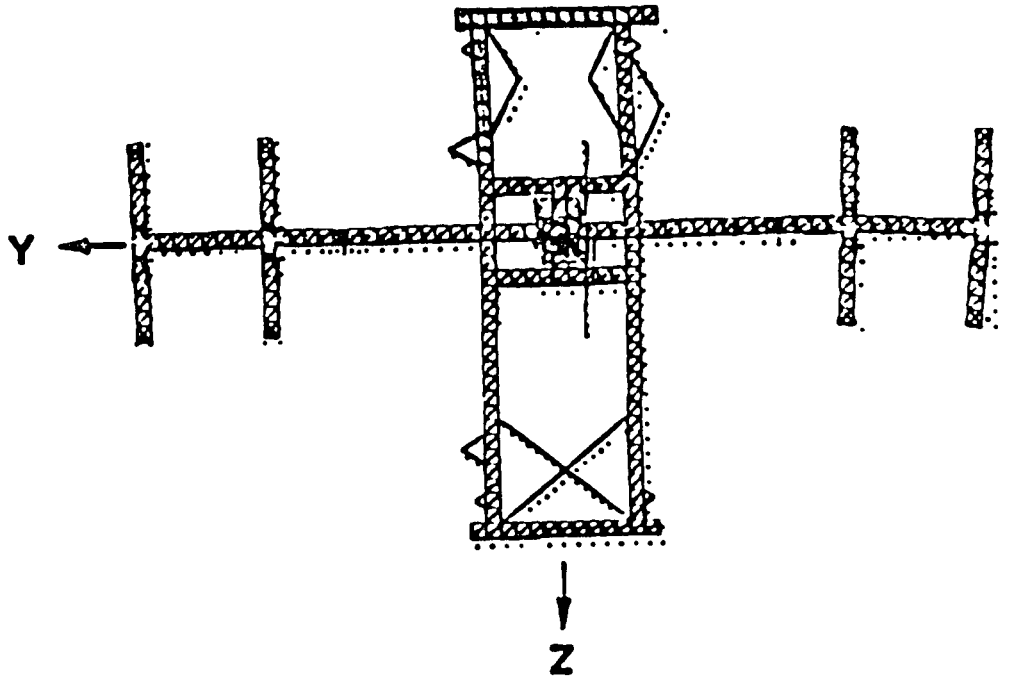

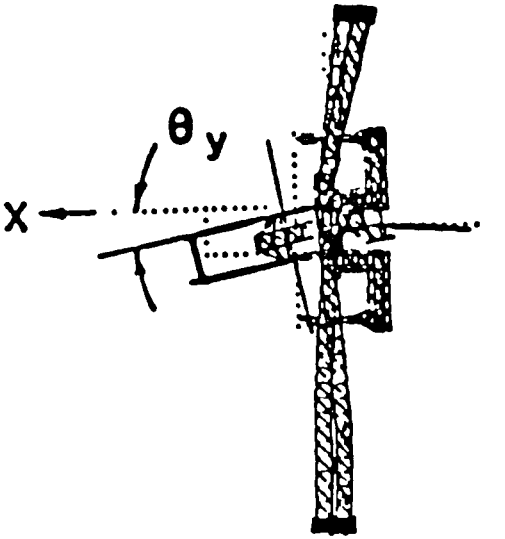

$f_{5\text{-meter}} = 0.339$ Hz

$f_{9\text{-foot}} = 0.185$ Hz

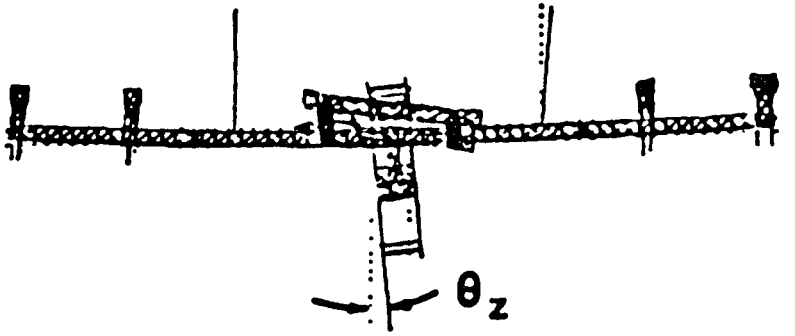

Figure 24.- Structural mode shape "M".

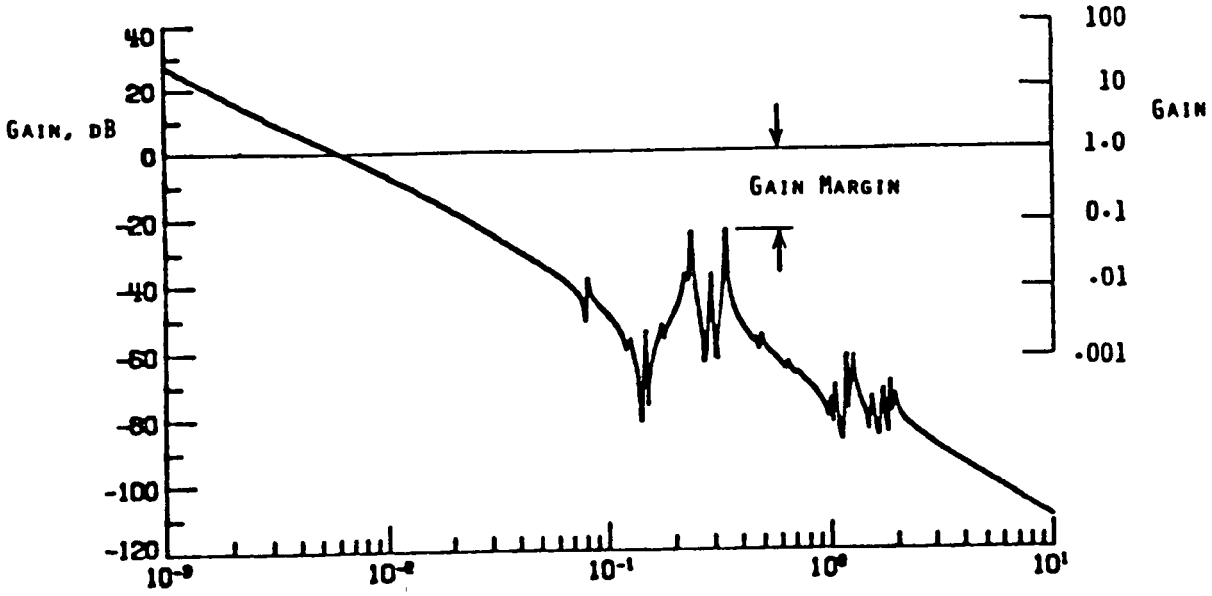

(a) Gain.

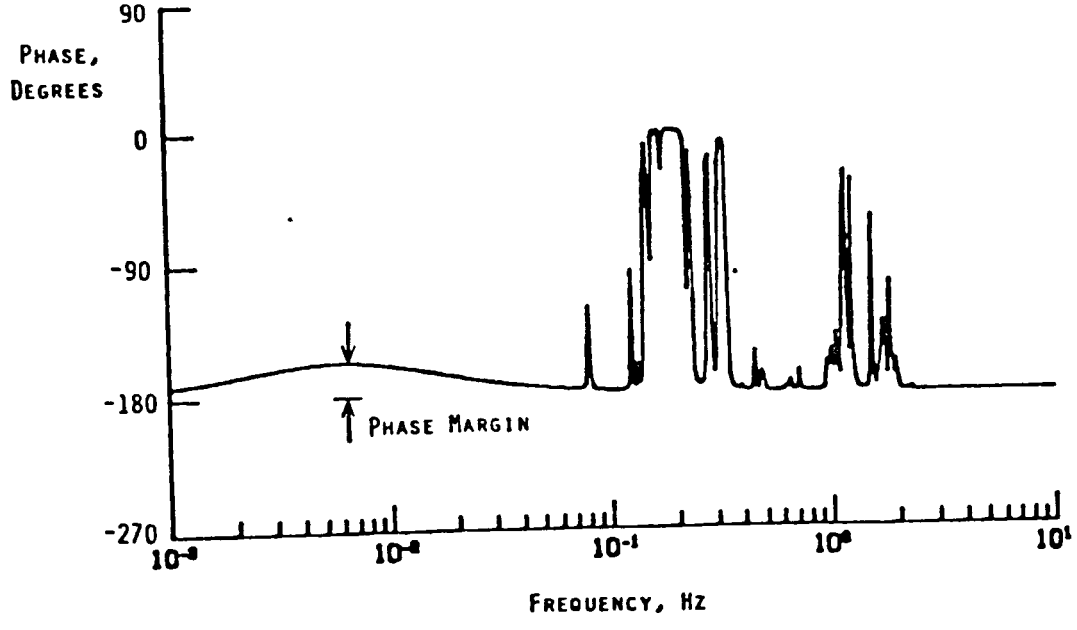

(b) Phase.

Figure 25.- Frequency response, 5-meter space station, compensated PD controller.

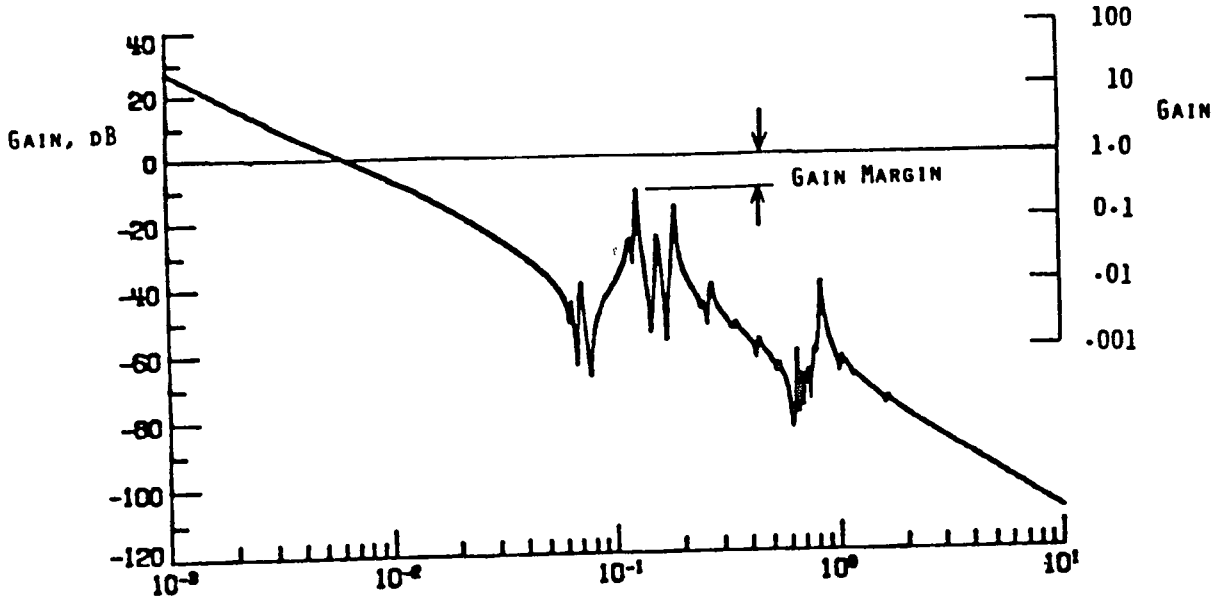

(a) Gain.

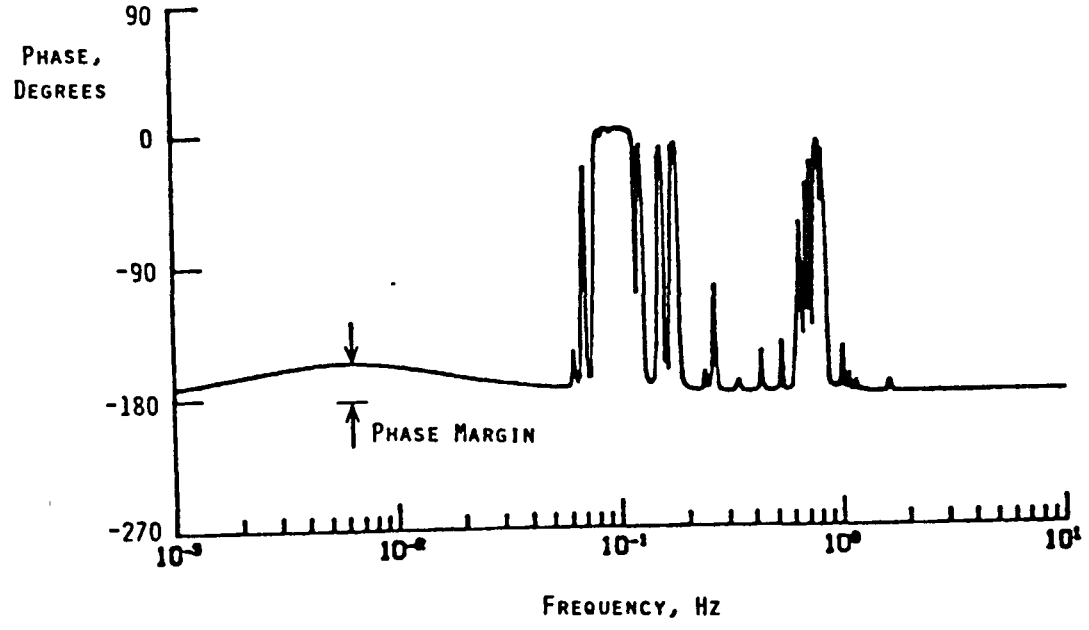

(b) Phase.

Figure 26.- Frequency response, 9-foot space station, compensated PD contoller.

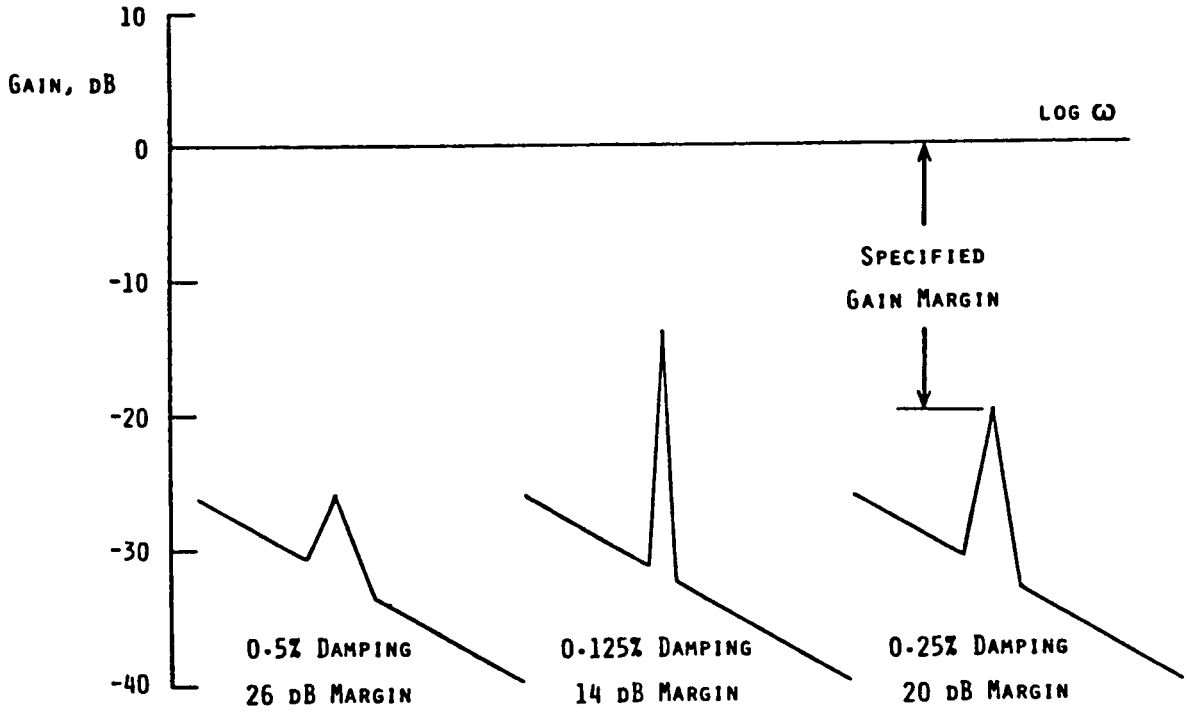

Figure 27.- Example illustrating relationship between gain margin and structural damping.

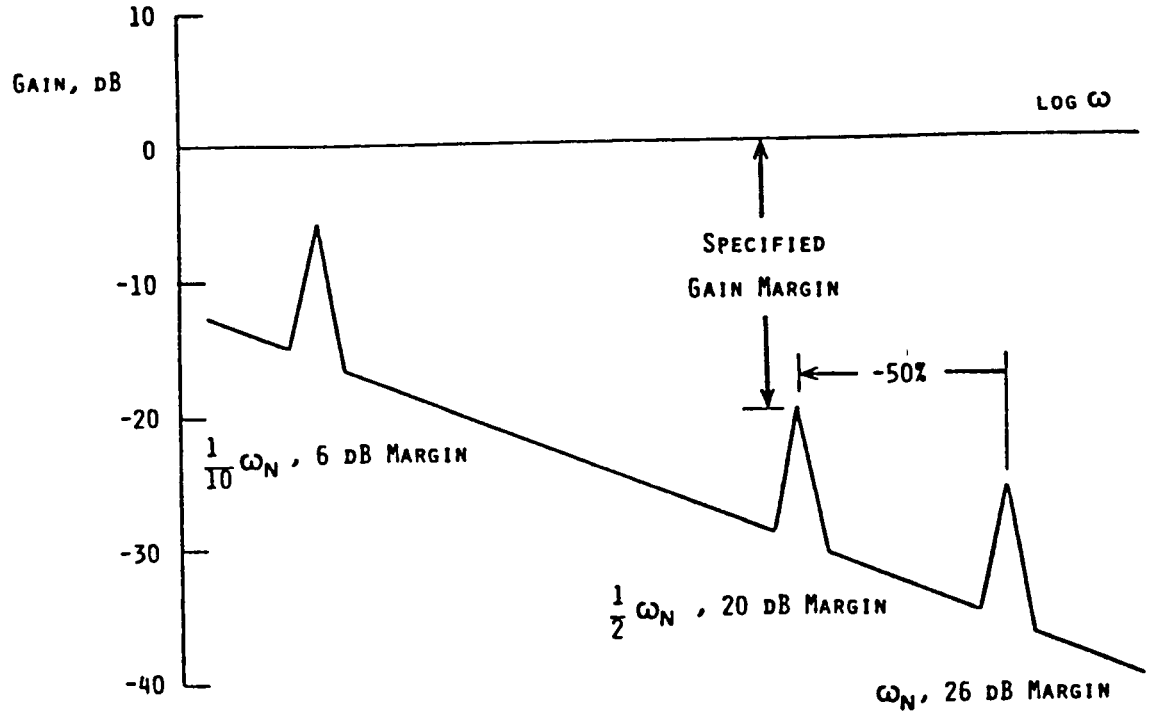

Figure 28.- Example illustrating relationship between gain margin and structural frequencies.

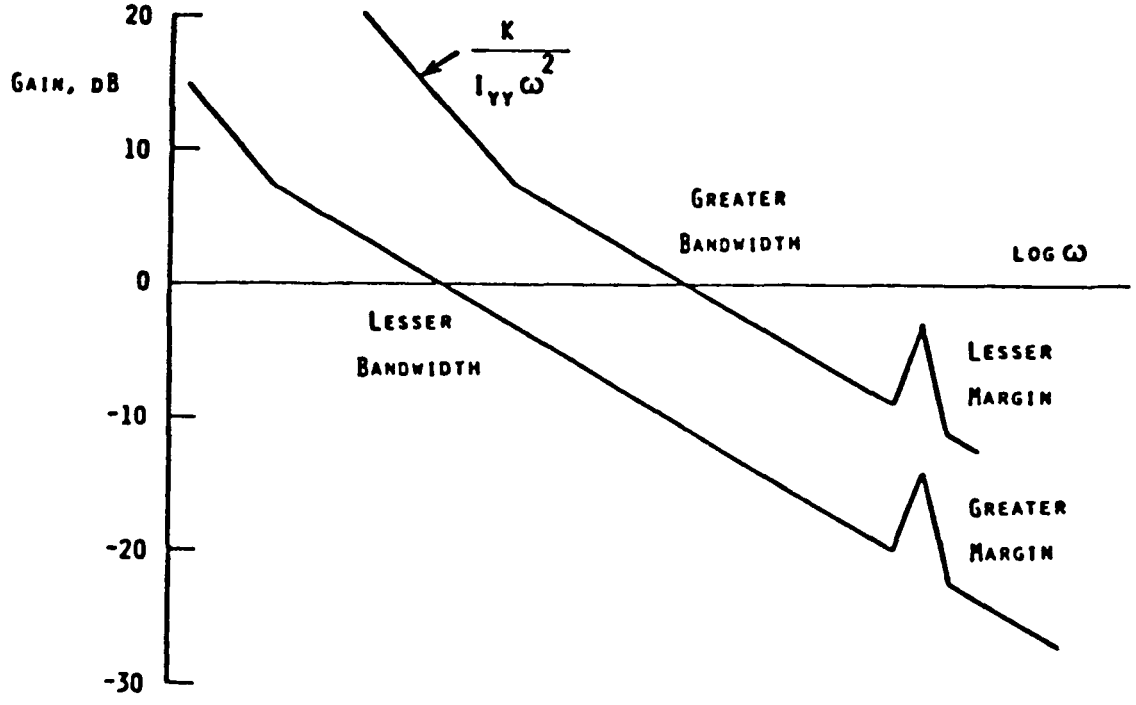

Figure 29.- Example Illustrating Relationship Between Gain Margin and System Bandwidth.

1 Report No	2 Government Accession No	3 Recipient's Catalog No
NASA TM-87679		

4 Title and Subtitle	5 Report Date
CONTROL/STRUCTURES INTERACTION STUDY OF TWO 300 KW DUAL-KEEL SPACE STATION CONCEPTS	May 1986
	6 Performing Organization Code 482-57-13-05
7 Author(s) John W. Young, Frederick J. Lallman, Paul A. Cooper, and Daniel P. Giesy*	8 Performing Organization Report No
	10 Work Unit No
9 Performing Organization Name and Address NASA Langley Research Center Hampton, VA 23665	11 Contract or Grant No
	13 Type of Report and Period Covered Technical Memorandum
12 Sponsoring Agency Name and Address National Aeronautics and Space Administration Washington, DC 20546	14 Sponsoring Agency Code

15 Supplementary Notes

*PRC Kentron, Inc., Hampton, Virginia.

16 Abstract

This paper presents the results of an investigation of the influence of structural stiffness of the space station framework on the controllability of two 300 kw class, solar dynamic powered, dual-keel space station designs. The two design concepts differed only in the truss bay dimensions of the structural framework of the stations. Two control studies were made; (1) A study of the interaction of the framework structural response with the reaction control system used for attitude control during an orbital reboost maneuver; and (2) A study of the stability of the space station attitude control system with sensors influenced by the elastic deformations of the station framework. Although both configurations had acceptable control characteristics, the configuration with the larger truss bay dimension and its increased structural stiffness had more attractive characteristics for pointing control of the solar dynamic system during reboost and for attitude control during normal in-orbit operations.

17 Key Words (Suggested by Author(s))	18 Distribution Statement
Space Station large space structures control/structures interaction	Unclassified--Unlimited Subject Category--18

19 Security Classif (of this report)	20 Security Classif (of this page)	21 No of Pages	22 Price
Unclassified	Unclassified	60	A04

N-305

For sale by the National Technical Information Service, Springfield, Virginia 22161

End of Document